cornea, type V collagen acts as a regulator of collagen fibril diameter; type V collagen forms collagen fibrils of small diameters by bonding with other types of collagen molecules.[40,41] Therefore, the increase in type V collagen ratio in the wound region might be necessary for formation and maintenance of collagen fibrils with uniform size.

To the best of our knowledge, this study is the first study in which atelocollagen was applied to a canine corneal wound. In the process of corneal stroma wound healing, scaffold selection is very important for keratocytes' effective proliferation.[42–44] The findings of the present study suggest that atelocollagen acted as scaffold of keratocyte proliferation. Consequently, in a naturally occurring wounded cornea, it is expected that filling the wound area of the corneal stroma with atelocollagen gel will support migration of keratocytes form the peripheral wound area and proliferation of keratocytes, and wound healing will thus be accelerated. It has been reported that transplantation of cells embedded in atelocollagen to defects of the dermis, cartilage, and bone showed good therapeutic results.[9,12,45–47] It was suggested that atelocollagen has a possibility as a matrix for repairing the corneal tissue. In the future, it will be necessary to evaluate the method by using more samples. In conclusion, this novel method using atelocollagen is advantageous for accelerating wound healing without causing inflammation.

Declaration of interest: The authors report no conflicts of interest. The authors alone are responsible for the content and writing of the paper.

REFERENCES

[1] Hansen PA, Guandalini A. A retrospective study of 30 cases of frozen lamellar corneal grafts in dogs and cats. *Vet Ophthalmol.* 1999;2:233–241.

[2] Kuchle M, Cursiefen C, Nguyen NX, Langenbucher A, Seitz B, Wenkel H, Martus P, Naumann GO. Risk factors for corneal allograft rejection: Intermediate results of a prospective normal-risk keratoplasty study. *Graefes Arch Clin Exp Ophthalmol.* 2002;240:580–584.

[3] Connon CJ, Meek KM. The structure and swelling of corneal scar tissue in penetrating full-thickness wounds. *Cornea.* 2004;23:165–171.

[4] Wilson SE, Kaufman HE. Graft failure after penetrating keratoplasty. *Surv Ophthalmol.* 1990;34:325–356.

[5] Whitley RD. Canine cornea. In: Gellat KN, ed. *Veterinary Ophthalmology.* 2nd ed. Philadelphia, PA: Lea and Fegiger; 1991:307–356.

[6] Shively JN, Epling GP. Fine structure of the canine eye: Cornea. *Am J Vet Res.* 1970;31:713–722.

[7] Samuelson DA. Ophthalmic embrology and anatomy. In: Gellat KN, ed. *Veterinary Ophthalmology.* 2nd ed. Philadelphia, PA: Lea and Fegiger; 1991:3–123.

[8] Ichioka S, Ohura N, Sekiya N, Shibata M, Nakatsuka T. Regenerative surgery for sacral pressure ulcers using collagen matrix substitute dermis (artificial dermis). *Ann Plast Surg.* 2003;51:383–389.

[9] Yamada N, Uchinuma E, Kuroyanagi Y. Clinical evaluation of an allogeneic cultured dermal substitute composed of fibroblasts within a spongy collagen matrix. *Scand J Plast Reconstr Surg Hand Surg.* 1999;33:147–154.

[10] Knapp TR, Kaplan EN, Daniels JR. Injectable collagen for soft tissue augmentation. *Plast Reconstr Surg.* 1977;60:398–405.

[11] Kojima K, Amano T. Injectable collagen for soft tissue contour defects. *J Transport Med.* 1985;39:6–13.

[12] Ono I, Zhou LJ, Tateshita T. Effects of a collagen matrix containing prostaglandin E(1) on wound contraction. *J Dermatol Sci.* 2001;25:106–115.

[13] Ono I, Tateshita T, Inoue M. Effects of a collagen matrix containing basic fibroblast growth factor on wound contraction. *J Biomed Mater Res.* 1999;48:621–630.

[14] Charriere G, Bejot M, Schnitzler L, Ville G, Hartmann DJ. Reactions to a bovine collagen implant. Clinical and immunologic study in 705 patients. *J Am Acad Dermatol.* 1989;21:1203–1208.

[15] Michelacci YM. Collagens and proteoglycans of the corneal extracellular matrix. *Braz J Med Biol Res.* 2003;36:1037–1046.

[16] Sakai J, Hung J, Zhu G, Katakami C, Boyce S, Kao WW. Collagen metabolism during healing of lacerated rabbit corneas. *Exp Eye Res.* 1991;52:237–244.

[17] Cintron C, Hong BS, Covington HI, Macarak EJ. Heterogeneity of collagens in rabbit cornea: Type III collagen. *Invest Ophthalmol Vis Sci.* 1988;29:767–775.

[18] Malley DS, Steinert RF, Puliafito CA, Dobi ET. Immunofluorescence study of corneal wound healing after excimer laser anterior keratectomy in the monkey eye. *Arch Ophthalmol.* 1990;108:1316–1322.

[19] SundarRaj N, Geiss III MJ, Fantes F, Hanna K, Anderson SC, Thompson KP, Thoft RA, Waring III GO. Healing of excimer laser ablated monkey corneas. An immunohistochemical evaluation. *Arch Ophthalmol.* 1990;108:1604–1610.

[20] Bailey AJ, Sims TJ, Le Lous, Bazin S. Collagen polymorphism in experimental granulation tissue. *Biochem Biophys Res Commun.* 1975;66:1160–1165.

[21] Gay S, Vijanto J, Raekallio J, Penttinen R. Collagen types in early phases of wound healing in children. *Acta Chir Scand.* 1978;144:205–211.

[22] Dahlgren LA, Brower-Toland BD, Nixon AJ. Cloning and expression of type III collagen in normal and injured tendons of horses. *Am J Vet Res.* 2005;66:266–270.

[23] Inoue M, Woo SLY, Gomez MA, Amiel D, Ohland KJ, Hitabayashi LR. Effect of surgical treatment and immobilization on the healing of the medial collateral ligament: A long-term multidisciplinary study. *Connect Tissue Res.* 1990;25:13–26.

[24] Hanada K, Shimazaki J, Shimmura S, Tsubota K. Multilayered amniotic membrane transplantation for severe ulceration of the cornea and sclera. *Am J Ophthalmol.* 2001;131:324–331.

[25] Gellat KN. Ophthalmic examination and diagnostic procedures. In: *Veterinary Ophthalmology,* 2nd ed. Philadelphia, PA: Lea and Fegiger; 1991:195–235.

[26] Sykes B, Francis MJ, Smith R. Altered relation of two collagen types in osteogenesis imperfecta. *N Engl J Med.* 1977;296:1200–1203.

[27] Agrawal VB, Tsai RJ. Corneal epithelial wound healing. *Ind J Ophthalmol.* 2003;51:5–15.

[28] Kenyon KR, Chaves HV. Morphology and pathologic response of corneal and conjunctival disease. In: Smolin G, Thoft RA, eds. *The Cornea,* 3rd ed. Boston, MA: Little, Brown and Company; 1994:69–111.

[29] Otori T. Electrolyte content of the rabbit corneal stroma. *Exp Eye Res.* 1967;6:356–367.

[30] Funderburgh JL, Funderburgh ML, Mann MM, Corpuz L, Roth MR. Proteoglycan expression during transforming growth factor beta-induced keratocyte-myofibroblast transdifferentiation. *J Biol Chem.* 2001;276:44173–44178.

[31] Kitano S, Goldman JN. Cytologic and histochemical changes in corneal wound repair. *Arch Ophthalmol*. 1966;76:345–354.
[32] Tanaka T. Comparison of stromal remodeling and keratocyte response after corneal incision and photorefractive keratectomy. *Jpn J Ophthalmol*. 2000;44:579–590.
[33] Hassell JR, Cintron C, Kublin C, Newsome DA. Proteoglycan changes during restoration of transparency in corneal scars. *Arch Biochem Biophys*. 1983;222:362–369.
[34] Assil KK, Quantock AJ. Wound healing in response to keratorefractive surgery. *Surv Ophthalmol*. 1993;38:289–302.
[35] Kato T, Nakayasu K, Kanai A. Corneal wound healing: Immunohistological features of extracellular matrix following penetrating keratoplasty in rabbits. *Jpn J Ophthalmol*. 2000;44:334–341.
[36] Niyibizi C, Kavalkovich K, Yamaji T, Woo SL. Type V collagen is increased during rabbit medial collateral ligament healing. *Knee Surg Sports Traumatol Arthrosc*. 2000;8:281–285.
[37] Shimomura T, Jia F, Niyibizi C, Woo SL. Antisense oligonucleotides reduce synthesis of procollagen alpha1 (V) chain in human patellar tendon fibroblasts: Potential application in healing ligaments and tendons. *Connect Tissue Res*. 2003;44:167–172.
[38] Hosaka Y, Ueda H, Yamasaki T, Suzuki D, Matsuda N, Takehana K. Structure and component alteration of rabbit Achilles tendon in tissue culture. *Biomed Res*. 2005;26:279–286.
[39] Yamamoto E, Hata D, Kobayashi A, Ueda H, Tangkawattana P, Oikawa M, Takehana K. Effect of beta-aminopropionitrile and hyaluronic acid on repair of collagenase-induced injury of the rabbit Achilles tendon. *J Comp Pathol*. 2002;126:161–170.
[40] Takemura Y, Mizuno K, Imamura Y, Hayashi T. Preferential liberation of type V collagen from bovine corneal stroma by limited treatment with proteases. *Connect Tissue*. 2003;35:133–139.
[41] Birk DE, Fitch JM, Babiarz JP, Doane KJ, Linsenmayer TF. Collagen fibrillogenesis *in vitro*: Interaction of types I and V collagen regulates fibril diameter. *J Cell Sci*. 1990;95:649–657.
[42] Doillon CJ, Watsky MA, Hakim M, Wang J, Munger R, Laycock N, Osborne R, Griffith M. A collagen-based scaffold for a tissue engineered human cornea: Physical and physiological properties. *Int J Artif Organs*. 2003;26:764–773.
[43] Vrana E, Builles N, Hindie M, Damour O, Aydinli A, Hasirci V. Contact guidance enhances the quality of a tissue engineered corneal stroma. *J Biomed Mater Res A*. 2008;84:454–463.
[44] Torbet J, Malbouyres M, Builles N, Justin V, Roulet M, Damour O, Oldberg A, Ruggiero F, Hulmes DJ. Orthogonal scaffold of magnetically aligned collagen lamellae for corneal stroma reconstruction. *Biomaterials*. 2007;28:4268–4276.
[45] Ito Y, Ochi M, Adachi N, Sugawara K, Yanada S, Ikada Y, Ronakorn P. Repair of osteochondral defect with tissue-engineered chondral plug in a rabbit model. *Arthroscopy*. 2005;21:1155–1163.
[46] Katsube K, Ochi M, Uchio Y, Maniwa S, Matsusaki M, Tobita M, Iwasa J. Repair of articular cartilage defects with cultured chondrocytes in Atelocollagen gel. Comparison with cultured chondrocytes in suspension. *Arch Orthop Trauma Surg*. 2000;120:121–127.
[47] Kimura A, Watanabe T, Shimizu T, Okafuji N, Mori R, Furusawa K, Kawai T, Hasegawa H, Kawakami T. Bone repair of rabbit mandibular transection using rhBMP-2 and atelocollagen gel. *Eur J Med Res*. 2006;11:355–358.

Available online at www.sciencedirect.com
ScienceDirect
Acta Biomaterialia 5 (2009) 470–476
Acta BIOMATERIALIA
www.elsevier.com/locate/actabiomat

Temperature-responsive glass coverslips with an ultrathin poly(*N*-isopropylacrylamide) layer

Kazuhiro Fukumori [a], Yoshikatsu Akiyama [b], Masayuki Yamato [b], Jun Kobayashi [b], Kiyotaka Sakai [a], Teruo Okano [b,*]

[a] *Department of Applied Chemistry, Waseda University, 3-4-1 Ohkubo, Shinjuku, Tokyo 169-8555, Japan*
[b] *Institute of Advanced Biomedical Engineering and Science, Tokyo Women's Medical University, 8-1 Kawadacho, Shinjuku, Tokyo 162-8666, Japan*

Received 4 February 2008; received in revised form 9 June 2008; accepted 13 June 2008
Available online 9 July 2008

Abstract

A temperature-responsive cross-linked polymer gel was covalently grafted onto glass coverslips by electron beam irradiation. The grafted thickness and amount of polymer as well as the surface wettability increased with the initial monomer concentration. When the monomer concentration was 5 wt.%, the grafted polymer density was 0.84 $\mu g\,cm^{-2}$, and cells adhered and spread on the surface at 37 °C, but detached at 20 °C. In contrast, when the monomer concentration was 35 wt.%, the polymer density was 1.28 $\mu g\,cm^{-2}$, and the surfaces were cell repellent even at 37 °C. These results show a remarkable contrast to those obtained from temperature-responsive polymer-grafted tissue culture polystyrene dishes, since various types of cells showed temperature-dependent cell adhesion/detachment when the grafted density was around 2 $\mu g\,cm^{-2}$ on these surfaces. We discuss the possible molecular mechanisms underlying this discrepancy.

Keywords: Poly(*N*-isopropylacrylamide) (PIPAAm); Electron beam; Cell adhesion; Cell detachment

1. Introduction

The temperature-responsive polymer, poly(*N*-isopropylacrylamide) (PIPAAm), possesses a lower critical solution temperature (LCST) of 32 °C in water [1]. Below the LCST, PIPAAm is fully hydrated and soluble in aqueous solution, but collapses extensively and becomes insoluble in the solution above the LCST. This unique feature of PIPAAm has been exploited for various biomedical applications [2–14], as has the use of PIPAAm's hydrophobic interactions with amino acids and proteins [15,16]. In our laboratory, chromatographic separation of a variety of bioactive molecules using the aqueous mobile phase could be achieved with temperature changes [5,6]. We have also utilized PIPAAm grafting into glass capillaries to make microfluidic valves [8]. In addition, by grafting polymer gel onto cell culture dishes using electron beam (EB) irradiation, temperature-dependent cell adhesion/detachment control could be achieved, with the development of temperature-responsive culture surfaces for tissue engineering and regenerative medicine applications [4,9–13]. In comparison to general polymerization methods, such as atom transfer radical polymerization [17] and chemical coupling [5,6], EB grafting techniques present several advantages. Using EB irradiation, it is relatively easy to graft polymer gel onto material surfaces, since no special initiators or catalysts are required and the polymerization reaction is carried out in an open system. Using EB irradiation, mass production of temperature-responsive culture dishes can be easily achieved. However, the thickness of the grafted polymer is a key factor in the control of cell adhesion/detachment in response to temperature. When PIPAAm is grafted onto tissue culture polystyrene (TCPS) dishes, a density of approximately 1.4 $\mu g\,cm^{-2}$ (ca. 20 nm in thickness) is optimal for the

* Corresponding author. Tel.: +81 3 3353 8112x66200; fax: +81 3 3359 6046.
E-mail address: tokano@abmes.twmu.ac.jp (T. Okano).

1742-7061/$ - see front matter © 2008 Acta Materialia Inc. Published by Elsevier Ltd. All rights reserved.
doi:10.1016/j.actbio.2008.06.018

temperature-responsive cell adhesion/detachment control of various types of cells [18]. The lower grafted density fails to enable cell detachment below the LCST. On the other hand, if the grafted density is higher than 1.4 g cm^{-2}, cells do not adhere on these surfaces even at 37 °C. The cell-repellent properties of PIPAAm grafted at higher densities can be explained by the interactions of the grafted polymer chains. In the PIPAAm-grafted layers, the polymer chains are dehydrated as they get progressively closer to the vicinity of hydrophobic TCPS, due to the restricted molecular motion of the grafted chains at the interfaces with the hydrophobic TCPS surfaces [18]. This hydrophobic property of the TCPS surfaces is also likely to promote the dehydration of the PIPAAm. At 37 °C, this effect promotes dehydration of the PIPAAm-grafted chains at the outermost surfaces, allowing for cell adhesion on the PIPAAm-grafted surfaces. When the graft thickness is increased, such progressive dehydration of the PIPAAm chains is weakened at the outermost portions of the PIPAAm chains and the surfaces fail to support cell adhesion [18]. In the present study, to investigate whether such phenomena as the thickness dependency of cell adhesion/detachment properties is observed for other substrate, we employed glass coverslips modified with 3-methacryloxypropyltrimethoxysilane (MPTMS) as the surfaces for PIPAAm-grafting. Temperature-dependent surface property changes of PIPAAm-grafted coverslips (PIPAAm-CSs) were examined in comparison to those of PIPAAm-grafted TCPS dishes (PIPAAm-TCPS).

2. Materials and methods

2.1. Reagents

N-Isopropylacrylamide (IPAAm) was kindly provided by Kohjin (Tokyo, Japan). The following materials were purchased from the respective companies: 3-methacryloxypropyltrimethoxysilane (MPTMS) from Sin-Etsu Chemical (Tokyo, Japan); 2-propanol from Kanto Chemical (Tokyo, Japan); methanol and toluene from Wako Pure Chemical Industries (Osaka, Japan); Dulbecco's modified Eagle's medium (DMEM) and Dulbecco's modified phosphate-buffered saline (PBS) from Sigma (St. Louis, MI); streptomycin and penicillin from GIBCO BRL (Gaithersburg, MD); fetal bovine serum (FBS) from Moregate Biotech (Australia); and bovine carotid artery endothelial cells (ECs) from Health Science Research Sources Bank (JCBR0099, Osaka, Japan).

2.2. Preparation of PIPAAm-grafted glass coverslip surfaces by electron beam irradiation

Glass coverslips (24 × 50 mm, 0.2 mm in thickness, from Matsunami Glass Inc., Osaka, Japan) were cleaned by oxygen plasma treatment and placed in a 500 ml separable flask with 3 ml of MPTMS. The coupling reaction of vaporized MPTMS with the coverslip surfaces (MPTMS-CS) was performed under N_2 gas at 70 °C for 3 h, as reported previously [19]. The coverslips were rinsed with toluene, methanol and distilled water, then dried for 3 h at 160 °C. IPAAm monomer in 2-propanol solution (to give a final monomer concentration of 5–50 wt.%) was spread onto silanized glass surfaces. The surfaces were then subjected to irradiation with 0.25 MGy electron beam (EB) using an area beam electron processing system (Nisshin High Voltage, Kyoto, Japan) and rinsed with cold distilled water to remove nongrafted IPAAm, PIPAAm and PIPAAm gel.

2.3. Characterization of poly(*N*-isopropylacrylamide)-grafted glass coverslips

The amount of the PIPAAm grafted onto the coverslips was determined by attenuated total reflection-fourier transform infrared spectroscopy (ATR-FTIR) (Spectrum One, Perkin Elmer Japan Co., Ltd., Kanagawa, Japan). As the base substrate was glass, a strong adsorption arising from Si–O was observed at 1000 cm^{-1} [20]. Adsorption of amide carbonyl derived from PIPAAm appeared in the region of 1650 cm^{-1}. The peak intensity ratio of I_{1650}/I_{1000} was used to determine the amount of PIPAAm grafted onto surfaces using a calibration curve prepared for a known amount of PIPAAm cast on MPTMS surfaces. The equation determined from the calibration curve was $y = 0.0147x - 0.0005$ where y is the grafted density of PIPAAm (μg cm^{-2}) and x is the peak intensity ratio of I_{1650}/I_{1000} ($R^2 = 0.989$). Samples were abbreviated as 0.84PIPAAm-CS (PIPAAm graft density = 0.84 μg cm^{-2}), 0.86PIPAAm-CS (0.86 μg cm^{-2}), 0.89PIPAAm-CS (0.89 μg cm^{-2}), 1.00PIPAAm-CS (1.00 μg cm^{-2}), 1.28PIPAAm-CS (1.28 μg cm^{-2}), 1.41PIPAAm-CS (1.41 μg cm^{-2}) and 1.49PIPAAm-CS (1.49 μg cm^{-2}). PIPAAm-TCPS were fabricated as reported previously [18], and abbreviated as 1.40PIPAAm-TCPS (1.40 μg cm^{-2}). PIPAAm-grafted surfaces were also examined by X-ray photoelectron spectroscopy (XPS) (JPS-9010TR, JOEL, Tokyo, Japan). Survey spectra were acquired at a take-off angle of 10–90° and surface elemental compositions were calculated using integrated peak areas. Contact angles of PIPAAm-CSs, MPTMS-CS and TCPS surfaces were determined by the captive bubble technique in Milli-Q water at 37 and 20 °C with a FACE contact angle meter (image processing type CA-X, Kyowa Interface Science, Saitama, Japan). Three samples were used for the determination, and each sample surface was measured at more than three points. Contact angles and the difference between those at 37 and 20 °C were represented as mean value and standard deviation. In order to evaluate the thickness of the grafted PIPAAm, the grafted PIPAAm was completely ablated to re-expose the glass surface with ArF excimer laser (wavelength = 193 nm, pulse width = 5 ns, laser fluence = 50 mJ cm^{-2}, no. of laser shots = 5) by passing a laser pulse through an optical microscope with a square photomask (L5910 IIIB, Ham-

amatsu Photonics, Shizuoka, Japan). The depth of the ablated domains was obtained by atomic force microscopy (AFM) (non-contact mode in air; SPM-9500J3, Shimadzu, Kyoto, Japan). The images presented were processed by flattening to remove the background slope using SPM software (SPM offline version 2.40; Shimadzu, Kyoto, Japan). Root mean square (RMS) values of the flattened images were further obtained using the software.

2.4. Cell adhesion and detachment assay

ECs were cultured on TCPS dishes (3001, Becton Dickinson, NJ) containing 5 ml of DMEM supplemented with 10% FBS, 100 units ml^{-1} penicillin and 100 μg ml^{-1} streptomycin at 37 °C under a humidified atmosphere with 5% CO_2 and 95% air. ECs in confluent cultures were harvested from TCPS dishes by treatment with 0.25% trypsin–0.26 mM EDTA in PBS for 5 min. ECs were seeded at a cell density of 1.0×10^4 cells cm^{-2} and cultured with DMEM supplemented with 10% FBS at 37 °C. Phase contrast microscopic images were acquired at designated time points, and the adherent cell number was counted in each image. For the detachment assay, culture surfaces were transferred to a CO_2 incubator set at 20 °C. Remaining adherent cell numbers on each surface were counted periodically.

3. Results and discussion

3.1. Surface characterization

The surface elemental composition was determined by XPS (Table 1). The high resolution C1s spectrum of 0.84PIPAAm-CS was modeled by superposition of the four peaks expected for PIPAAm, resulting in a very close match to the experimentally observed spectrum (Fig. 1). The sp^2-hybridized carbon atom in the carbonyl group, labeled IV, peaked at 287.9 eV and had an integrated molar ratio of 16.2%, which is very close to the expected value (16.7%). The sp^3-hybridized carbon peak at 285.0 eV was divided into three components: peak I at 284.9 eV, corresponding to the two CH_3- groups in the isopropyl group and the -CH_2- in the PIPAAm backbone; peak II at 285.3 eV, attributable to the -CH- unit in the PIPAAm backbone; and peak III at 286.2 eV, corresponding to the -CH- unit adjacent to -NH- group. The molar ratios for the three peaks, I, II and III, were 51.6, 14.9 and 17.3%, respectively, matching those for the three peaks of the ideal chemical composition of PIPAAm (I:II:III = 50.0:16.7:16.7%). The atomic composition, carbon, oxygen and nitrogen of 0.84PIPAAm-CS as well as the atomic ratio of N/C are in good agreement with those predicted from the stoichiometry of the IPAAm monomer. They were also consistent with those of PIPAAm-TCPS. The relative atomic composition of carbon and nitrogen increased from 37.6 to 73.1 and from 2.7 to 13.4, while that of oxygen and silicon decrease dramatically from 41.1 to 12.5 and from 18.6 to 1.1. These results illustrate that the grafted PIPAAm gel fully covered the coverslip surfaces. FTIR spectra of 0.84PIPAAm-CS showed characteristic bands for the grafted PIPAAm (C=O at 1650 cm^{-1}, C–H at 2980 cm^{-1} and N–H at 3300 cm^{-1}) and for basal glass coverslips (Si–O–Si at 1000 cm^{-1}, hydrogen bonded Si–OH at 3480 cm^{-1}) [20], suggesting that silanol groups remain on the basal glass coverslip surfaces after MPTMS treatment and EB irradiation. Namely, PIPAAm gel is suc-

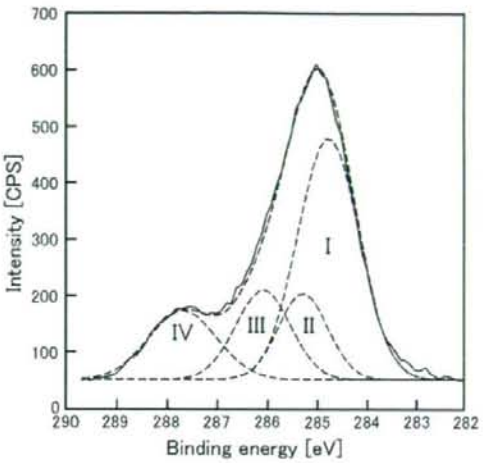

Fig. 1. High-resolution XPS C1s spectrum of 0.84PIPAAm-CS. The solid curve is the experimental data and the dashed curves are the fitted curves.

Table 1
Atomic compositions of PIPAAm-CSs determined by XPS

		Relative atomic composition (%)				Atomic ratio
	Take off angle	C	N	O	Si	N/C
MPTMS-CS	90°	37.6	2.7	41.1	18.6	–
0.84PIPAAm-CS	10°	73.1	13.4	12.5	1.1	0.18
0.84PIPAAm-CS	50°	64.2	12.1	16.6	7.1	0.19
0.84PIPAAm-CS	90°	59.9	12.1	19.3	8.7	0.20
1.40PIPAAm-TCPS	10°	78.1	10.5	10.8	0.6	0.13
IPAAm-monomer[a]	–	75.0	12.5	12.5	–	0.17

[a] Atomic composition was calculated from ideal IPAAm monomer.

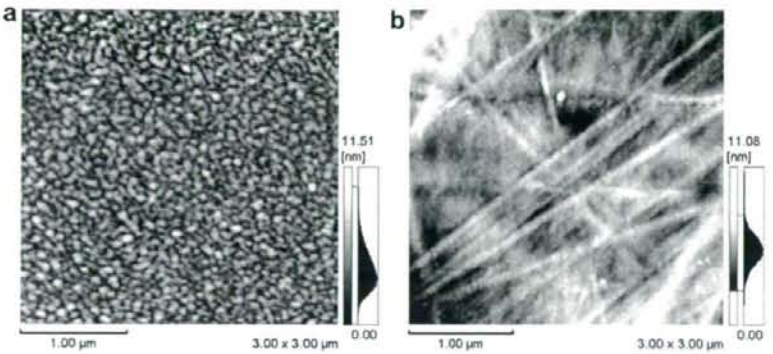

Fig. 2. AFM images of (a) 0.84PIPAAm-CS and (b) 1.40PIPAAm-TCPS surfaces.

cessfully grafted onto the glass surfaces with the remaining silanol groups.

AFM revealed that 0.84PIPAAm-CS surfaces uniformly exhibited a domain-like structure of ca. 70–100 nm (Fig. 2(a)), while the 1.40PIPAAm-TCPS had a smaller sized domain-like structure than 0.84PIPAAm-CS (ca. 20–30 nm) (Fig. 2(b)). The stripe and groove texture observed in Fig. 2(b) is made during the production process of TCPS [21]. The resulting domain-like structure implies phase separation during EB irradiation, as mentioned in a previous report [21]. Regardless of the initial IPAAm concentration, the size of the former domain-like structure remained roughly the same, and was relatively larger than those observed with 1.40PIPAAm-TCPS. The different sizes of the domain-like structure might be ascribed to the different numbers of graft initiating points and the different reactivity of the functional groups between MPTMS-modified glass and TCPS surfaces. The degree of roughness of the surfaces is often denoted as RMS values [22,23], and has an influence on the cell adhesion properties of the surfaces [24–26]. RMS values of 0.84PIPAAm-CS and 1.40PIPAAm-TCPS were mutually equivalent (1.67 nm for 0.84PIPAAm-CS and 2.38 nm for 1.40PIPAAm-TCPS), indicating that an effect of roughness of the two surfaces on cell adhesion behavior is negligible.

Table 2
Characterizations of PIPAAm-CSs and PIPAAm-TCPS

Initial monomer concentration (wt.%)[a]	Amount of grafted PIPAAm (μg/cm^2)	PIPAAm Thickness (nm)	Abbreviation
5	0.84 ± 0.03	3.5 ± 0.2	0.84PIPAAm-CS
10	0.86 ± 0.11	4.1 ± 0.2	0.86PIPAAm-CS
20	0.89 ± 0.08	4.4 ± 0.4	0.89PIPAAm-CS
30	1.00 ± 0.09	4.8 ± 0.1	1.00PIPAAm-CS
35	1.28 ± 0.08	7.4 ± 0.3	1.28PIPAAm-CS
40	1.41 ± 0.02	8.8 ± 0.4	1.41PIPAAm-CS
50	1.49 ± 0.07	9.6 ± 0.6	1.49PIPAAm-CS
55[b]	1.40 ± 0.10	15.5 ± 7.2	1.40PIPAAm-TCPS

[a] 2-Propanol was used as solvent.
[b] TCPS was used as basal substrate [14].

The thickness of the grafted PIPAAm layers on the PIPAAm-CS surfaces prepared with different initial monomer concentrations was evaluated with selective ultraviolet laser ablation of the polymer layer and AFM (Table 2, Fig. 3). A significant increase in the amount and thickness of the grafted PIPAAm was observed above 30 wt.% IPAAm concentration. An adequate monomer concentration might improve the reaction efficiency of the MPTMS groups with IPAAm monomer and/or that among IPAAm monomers, consequently increasing the amount and thickness of the grafted PIPAAm. The density of the grafted PIPAAm layer was estimated roughly to be ca. 1.6 g cm^{-3} for 1.49PIPAAm-CS and ca. 2.4 g cm^{-3} for 0.84PIPAAm-CS from the amount and the thickness of grafted PIPAAm. Interestingly, a higher density of grafted PIPAAm was obtained with the thinner PIPAAm layers. Furthermore, the estimated

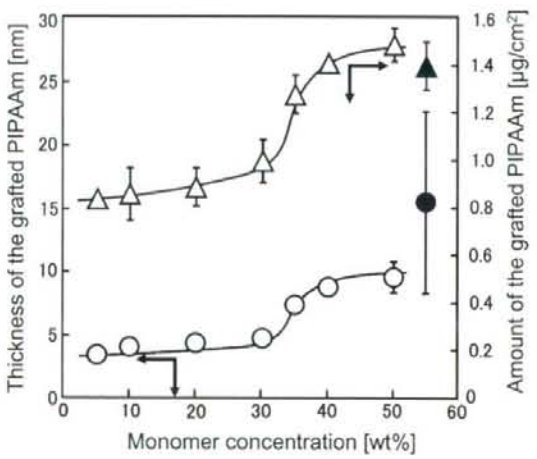

Fig. 3. Thickness and amount of grafted PIPAAm of PIPAAm-CSs (○,△) as a function of the initial monomer concentration. The corresponding values for 1.40PIPAAm-TCPS (●, ▲) are shown for comparison. Some error bars are smaller than the size of the symbols. The value for each error bar is shown in Table 2.

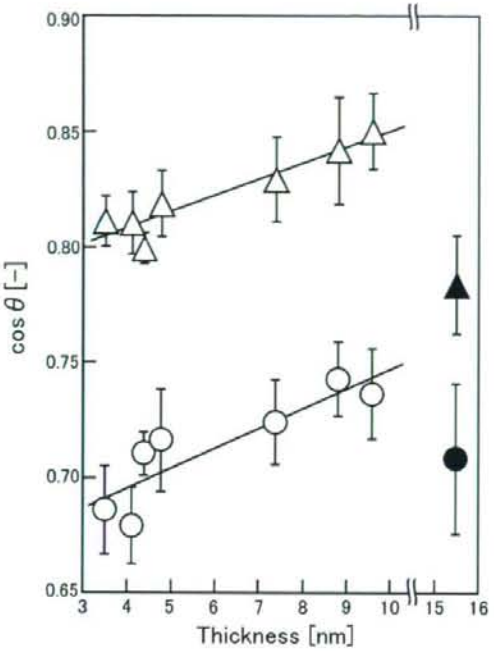

Fig. 4. Contact angles (cosθ values) of PIPAAm-CSs as a function of the thickness of the grafted PIPAAm at 37 °C (○) and 20 °C (△). 1.40PIPAAm-TCPS was employed for comparison (37 °C: ●; 20 °C: ▲).

PIPAAm density of PIPAAm-CSs is larger than those of PIPAAm-TCPS (ca. 1.0 g cm^{-3}) and typical synthetic polymers (ca. 1.0 g cm^{-3}). Taken together, the grafted PIPAAm chains of 0.84PIPAAm-CS are extremely compacted.

The wettability of the PIPAAm-CSs surfaces under aqueous conditions was evaluated with a captive bubble method at 20 and 37 °C (Fig. 4). Each PIPAAm-CS surface exhibited lower $\cos\theta$ values (more hydrophobic property) at 37 °C than at 20 °C, while wettability of the MTPMS-CS surface was independent of temperature ($\cos\theta = 0.39 \pm 0.03$ (20 °C) and 0.35 ± 0.03 (37 °C)). The wettability of the PIPAAm-CS surfaces increased with increasing thickness and amount of grafted PIPAAm (Fig. 4), coinciding with the observation obtained with PIPAAm-TCPS, in which the thickness and amount of grafted PIPAAm influenced the behavior of the top surfaces of the grafted PIPAAm layers [18,21,27]. Surprisingly, the wettability of 0.84PIPAAm-CS at 20 and 37 °C was similar to that of the 1.40PIPAAm-TCPS surfaces, which facilitate temperature-responsive cell adhesion/detachment control, respectively, while the amount and thickness of PIPAAm-CSs was significantly lower than those of 1.40PIPAAm-TCPS.

3.2. Cell adhesion and detachment

PIPAAm-CS surfaces were tested with the cell adhesion/detachment assay (Figs. 5 and 6). Cells adhered and spread well on MPTMS and 0.84PIPAAm-CS at 37 °C, but cell adhesion was diminished with increasing amount of grafted PIPAAm. 1.28PIPAAm-CS, 1.41PIPAAm-CS and 1.49PIPAAm-CS surfaces were cell-repellent.

After culture for 24 h at 37 °C, cultured cells were detached from 0.84PIPAAm-CS, 0.89PIPAAm-CS and 1.00PIPAAm-CS by lowering the temperature to 20 °C (Fig. 6). All the adhered cells were detached from 0.84PIPAAm-CS, 0.89PIPAAm-CS and 1.00PIPAAm-CS within 60 min at 20 °C, while approximately 80% of the adhered cells remained on MPTMS-CS even after 120 min at 20 °C. However, a slower cell detachment after lowering the temperature was observed with 1.40PIPAAm-TCPS. Endothelial cells proliferated and reached confluency on 0.84PIPAAm-CS in the presence of 10% FBS. By reducing the temperature to 20 °C, all the confluent cells were harvested as a single contiguous cell sheet (data not shown).

3.3. Comparison of surfaces properties dependent on the thickness and density of the grafted PIPAAm of PIPAAm-CSs with those of the PIPAAm-TCPS system

Fig. 7 shows the correlation between cell adhesion properties and the thickness of the grafted PIPAAm, clearly showing that PIPAAm-CSs with grafted PIPAAm of more than 1.28 μg cm^{-2} density and more than 7.4 nm thickness exhibited non-cell adhesive surfaces. Namely, the PIPAAm-CSs system also exhibited the PIPAAm thickness dependency of cell adhesion/detachment observed in the PIPAAm-TCPS system [18]. The boundary line of the PIPAAm-CSs system, which dominates following a cell adhesion event, appears to be relatively lower than PIPAAm-TCPS system (the boundary line appears between 15.5 ± 7.2 and 29.5 ± 8.4 nm) [18].

In our previous reports, the configuration and resulting dynamic motion of the grafted PIPAAm chains significantly influenced surface wettability in response to temperature change [2,3]. For ultrathin PIPAAm layers, the basal surface properties are also likely to influence the grafted PIPAAm chains, as described in our previous report [18]. The grafted PIPAAm chains in the vicinity of the hydrophobic TCPS interfaces not only have restricted molecular motion but are also dehydrated due to the basal hydrophobic property. PIPAAm chains at the outermost surfaces also suffer from progressive dehydration, and consequently fibronectin proteins contained in the FBS component should be adsorbed onto the surfaces. The cell adhesive properties are due to the adsorption of fibronectin (FN) molecules onto the thin layer [18]. However, for thicker PIPAAm layers, there is much less progressive dehydration at the outermost surfaces, and as a result the surfaces are cell repellent [18]. In fact, FN molecules were not adsorbed onto the thicker layer [18]. In contrast, a previous report has suggested that PIPAAm was not likely to be hydrophobic enough to interact with proteins even above the LCST [15]. This phenomenon may be due to the adequate hydration of PIPAAm chains even above the LCST [28]. The fact

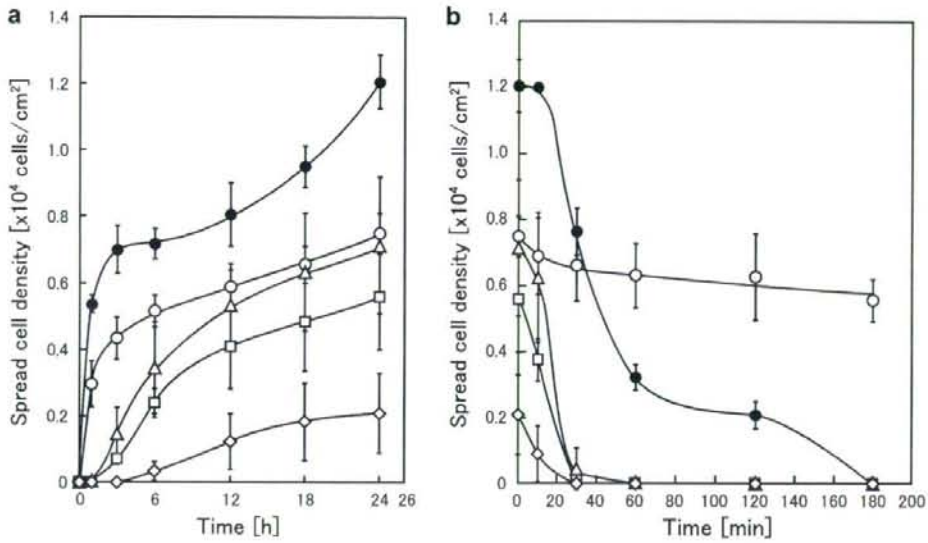

Fig. 5. Time-dependent cell attachment (a) and detachment (b) from MPTMS, PIPAAm-CSs and 1.40PIPAAm-TCPS by low-temperature treatment at 20 °C after culture for 24 h at 37 °C. ●: 1.40PIPAAm-TCPS; ○: MPTMS; △: 0.84PIPAAAm-CS; □: 0.89PIPAAm-CS; ◇: 1.00 PIPAAm-CS. Data are expressed as the mean with the standard error of the mean ($n > 3$). Initial cell density: 1×10^4 cells cm^{-2}.

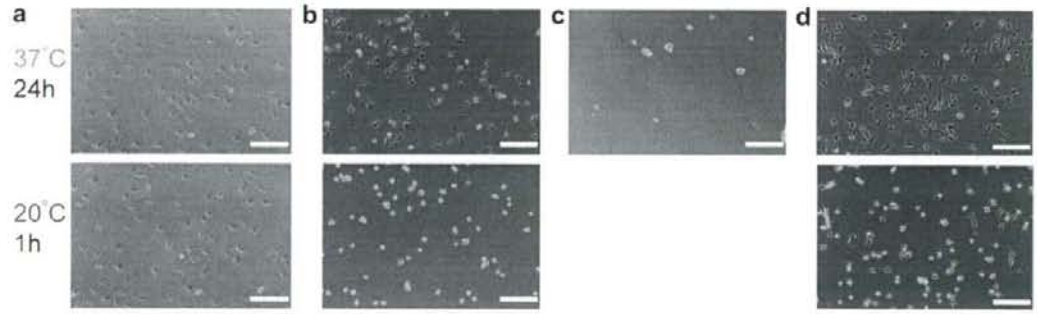

Fig. 6. Phase-contrast photographs of ECs cultured onto (a) MPTMS-CS, (b) 0.84PIPAAm-CS, (c) 1.41PIPAAm-CS and (d) 1.40PIPAAm-TCPS at 37 °C for 24 h (upper) and at 20 °C for 1 h (bottom). Scale bars = 200 μm.

that FN molecules were not adsorbed onto the thicker layer could possibly be ascribed to the adequate hydration of the grafted PIPAAm chains at the outermost surfaces, while adsorption of FN molecules onto the thin PIPAAm layer resulted from the progressive dehydration of the grafted PIPAAm chains. This consideration can be applied to the present PIPAAm-CSs system. However, for glass surfaces, less dehydration of the grafted PIPAAm chains at the interface of the glass is expected, like the hydrophobic TCPS one, due to the presence of remaining hydrophilic silanol groups. To compensate for this drawback, as shown in 0.84PIPAAm-CS, a more dense, thinner layer of the grafted PIPAAm may be necessary to promote the restriction of molecular motion of the grafted PIPAAm chains and to exhibit cell attachment/detachment properties in response to a change in temperature. We assume that the boundary line of the PIPAAm-CSs system being lower than that of the PIPAAm-TCPS system is attributable to the remaining silanol groups and the greater density of the grafted PIPAAm layer.

In conclusion, we have clearly shown that the thickness and amount of grafted PIPAAm have a significant influence on cell adhesion and detachment properties, as well as on surface properties. We have discussed the thickness dependency of these properties in terms of molecular motion of the grafted PIPAAm chains, comparing PIPAAm-CSs with PIPAAm-TCPS. Control of the thickness and density of the grafted PIPAAm chains is important for PIPAAm-CSs to exhibit cell attachment and detachment behavior in response to temperature. Presumably,

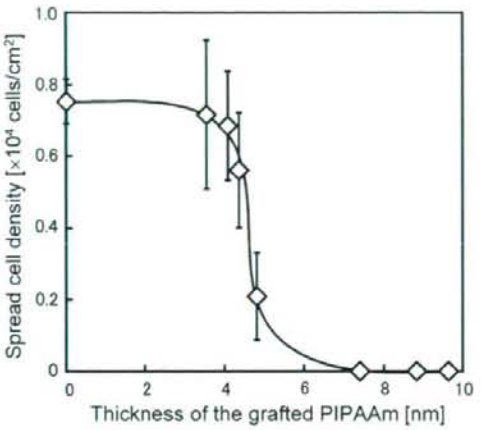

Fig. 7. Cells adhesive properties dependent on the thickness of the grafted PIPAAm.

the fact that PIPAAm layer of 0.84PIPAAm-CS is thinner than that of 1.40PIPAAm-TCPS is a result of the remaining silanol groups and the greater density of the grafted PIPAAm layer.

Acknowledgements

This work was supported by a Grant-in-Aid for Scientific Research on Priority Area (Grant No. 17076014), the Ministry of Education, Culture, Sports, Science and Technology (MEXT), Japan. This work is also done at the "Center for Practical Chemical Wisdom" supported by Global COE program of MEXT.

References

[1] Schild HG. Poly(*N*-isopropylacrylamide): experiment, theory and application. Prog Polym Sci 1992;17:163–249.
[2] Yakushiji T, Sakai K, Kikuchi A, Aoyagi T, Sakurai Y, Okano T. Graft architectural effects on thermoresponsive wettability changes of poly(*N*-isopropylacrylamide)-modified surfaces. Langmuir 1998;14:4657–62.
[3] Takei YG, Aoki T, Sanui K, Ogata N, Sakurai Y, Okano T. Dynamic contact angle measurement of temperature-responsive surface properties for poly(*N*-isopropylacrylamide) grafted surfaces. Macromolecules 1994;27:6163–6.
[4] Yamada N, Okano T, Sakai H, Karikusa F, Sawasaki Y, Sakurai Y. Thermo-responsive polymeric surfaces; control of attachment and detachment of cultured cells. Makromol Chem Rapid Commun 1990;11:571–6.
[5] Kanazawa H, Yamamoto K, Matsushima Y, Takai N, Kikuchi A, Sakurai Y, et al. Temperature-responsive chromatography using poly(*N*-isopropylacrylamide)-modified silica. Anal Chem 1996;68:100–5.
[6] Yakushiji T, Sakai K, Kikuchi A, Aoyagi T, Sakurai Y, Okano T. Effects of cross-linked structure on temperature-responsive hydrophobic interaction of poly(*N*-isopropylacrylamide) hydrogel-modified surfaces with steroids. Anal Chem 1999;71:1125–30.
[7] Idota N, Kikuchi A, Kobayashi J, Akiyama Y, Sakai K, Okano T. Thermal modulated interaction of aqueous steroids using polymer-grafted capillaries. Langmuir 2006;22:425–30.
[8] Idota N, Kikuchi A, Kobayashi J, Sakai K, Okano T. Microfluidic valves comprising nanolayered thermoresponsive polymer-grafted capillaries. Adv Mater 2005;17:2723–7.
[9] Yamato M, Akiyama Y, Kobayashi J, Yang J, Kikuchi A, Okano T. Temperature-responsive cell culture surfaces for regenerative medicine with cell sheet engineering. Prog Polym Sci 2007;32(8-9):1123–33.
[10] Nishida K, Yamato M, Hayashida Y, Watanabe K, Yamamoto K, Adachi E, et al. Corneal reconstruction with tissue-engineered cell sheets composed of autologous oral mucosal epithelium. N Engl J Med 2004;351:1187–96.
[11] Yang J, Yamato M, Kohno C, Nishimoto A, Sekine H, Fukai F, et al. Cell sheet engineering: recreating tissues without biodegradable scaffolds. Biomaterials 2005;26:6415–22.
[12] Kikuchi A, Okano T. Nanostructured designs of biomedical materials: applications of cell sheet engineering to functional regenerative tissues and organs. J Control Release 2005;101(3):69–84.
[13] Ohashi K, Yokoyama T, Yamato M, Kuge H, Kanehiro H, Tsutsumi M, et al. Engineering functional two- and three-dimensional liver systems in vivo using hepatic tissue sheets. Nat Med 2007;13:880–5.
[14] Gewehr M, Nakamura K, Ise M. Gel permeation chromatography using porous glass beads modified with temperature-responsive polymers. Makromol Chem 1992;193:249–56.
[15] Ivanov AE, Zhigis LS, Kurganova EV, Zubov VP. Effect of temperature upon the chromatography of proteins on porous glass, chemically coated with *N*-isopropylacrylamide copolymer. J Chromatogr A 1997;776:75–80.
[16] Bianco-Peled H, Gryc S. Binding of amino to smart sorbents: where does hydrophobicity come into play? Langmuir 2004;20:169–74.
[17] Matyjaszewski K, Xia J. Atom transfer radical polymerization. Chem Rev 2001;101:2921–90.
[18] Akiyama Y, Kikuchi A, Yamato M, Okano T. Ultrathin poly(*N*-isopropylacrylamide) grafted layer on polystyrene surfaces for cell adhesion/detachment control. Langmuir 2004;20:5506–11.
[19] Okusa H, Kurihara K, Kunitake T. Chemical modification of molecularly smooth mica surface and protein attachment. Langmuir 1994;10:3577–81.
[20] Fu Q, Rao GV, Ward TL, Lu Y, Lopez GP. Thermoresponsive transport through ordered mesoporous silica/PNIPAAm copolymer membrane and microspheres. Langmuir 2007;23:170–4.
[21] Akiyama Y, Kushida A, Yamato M, Kikuchi A, Okano T. Surface characterization of poly(*N*-isopropylacrylamide) grafted tissue culture polystyrene by electron beam irradiation, using atomic force microscopy, and X-ray photoelectron spectroscopy. J Nanosci Nanotechnol 2007;7:796–802.
[22] Namba Y, Yu J, Bennett MB, Yamashita K. Modeling and measurements of atomic surface roughness. Appl Optics 2000;39:2705–18.
[23] Teare DOH, Emmison N, Ton-That C, Bradley RH. Cellular attachment to ultraviolet ozone modified polystyrene surfaces. Langmuir 2000;16:2818–24.
[24] Thapa A, Miller DC, Webster TJ, Haberstroh KM. Nano-structured polymers enhance bladder smooth muscle cell function. Biomaterials 2003;24:2915–26.
[25] Thapa A, Webster TJ, Haberstroh KM. Polymers with nano-dimensional surface features enhance bladder smooth muscle cell adhesion. J Biomed Mater Res A 2003;67:1374–83.
[26] Chung TW, Liu DZ, Wang SY, Wang SS. Enhancement of the growth of human endothelial cells by surface roughness at nanometer scale. Biomaterials 2003;24:4655–61.
[27] Sakai H, Doi Y, Okano T, Yamada N, Sakurai Y. In: Ogata N, Feijin J, Kim SW, Okano T, editors. Advanced biomaterials in biomedical engineering and drug delivery systems. Tokyo: Springer; 1996. p. 229–30.
[28] Maeda Y, Higuchi T, Ikeda I. Change in hydration state during the coil-globule transition of aqueous solutions of poly(*N*-isopropylacrylamide) as evidenced by FTIR spectroscopy. Langmuir 2000;16:7503–9.

Biomaterials 29 (2008) 3650–3655

Contents lists available at ScienceDirect

Biomaterials

journal homepage: www.elsevier.com/locate/biomaterials

The effect of extensible PEG tethers on shielding between grafted thermo-responsive polymer chains and integrin–RGD binding

Mitsuhiro Ebara [a], Masayuki Yamato [b], Takao Aoyagi [b], Akihiko Kikuchi [b], Kiyotaka Sakai [a], Teruo Okano [b,*]

[a] Department of Applied Chemistry, Waseda University, 3-4-1 Ohkubo, Shinjuku-ku, Tokyo 169-8555, Japan
[b] Institute of Advanced Biomedical Engineering and Science, Tokyo Women's Medical University, 8-1 Kawada-cho, Shinjuku-ku, Tokyo 162-8666, Japan

ARTICLE INFO

Article history:
Received 17 January 2008
Accepted 27 May 2008
Available online 25 June 2008

Keywords:
Poly(*N*-isopropylacrylamide)
2-Carboxyisopropylacrylamide
Temperature-responsive surface
RGD peptides
Affinity control

ABSTRACT

The affinity control of integrin–RGD (Arg-Gly-Asp) binding by a thermal "on–off" switch has been achieved using newly designed surfaces presenting grafted temperature-responsive poly(*N*-isopropylacrylamide-*co*-2-carboxyisopropylacrylamide) copolymers functionalized with synthetic peptides. The prepared surface was designed to expose the tethered peptides available for cell binding at active "on" state above the lower critical solution temperature (LCST). The fully extended chains, on the other hand, masked the peptides completely and the cells started to detach from the surfaces at inactive "off" sate below the LCST. This paper elucidates the shielding effect of the grafted polymer chains on the dissociation of integrin–RGD binding below the LCST. To assess the ability of the polymer-shielding, extensible poly(ethylene glycol) (PEG) tethers were introduced between peptides and the grafted polymers. PEG chains allow peptides to be tethered to surfaces via functional PEG end-groups, leading to active "on" state even below the LCST. The time required to release cells from the surface was found to be longer when peptides were coupled to an extensible tether ends, suggesting that the surfaces can engender cell attachment through adhesive moieties covalently bound to the free ends of PEG chains. These results indicate that architectural changes on the nanometer length scale are crucial for controlling integrin–RGD binding and one of the main factors causing cell detachment is the shielding effect of the grafted polymer chains.

1. Introduction

Many biological and physiological processes in our body rely on affinity changes between bioactive molecules including ligand–receptor recognitions [1–3]. Cell membrane proteins, for example, regulate fundamental cellular processes such as cell adhesion, migration, proliferation, and differentiation by modulating the binding affinity with their ligand proteins, changing their conformations from inactive "off" state to active "on" state [4,5]. Binding of integrins to fibronectin (FN) triggers subsequent signal-transduction pathways, including clustering of integrin molecules, accumulation of cytoskeletal molecules, and assembly of soluble FN (FN polymerization) state [6–10]. In this way, cells regulate the multiple interactions with respect to inter/intra cellular signaling by changing the molecular conformation.

Several attempts have been made to control ligand–receptor recognitions using stimuli-responsive polymers [11–13]. Temperature-responsive poly(*N*-isopropylacrylamide) (PIPAAm) collapses from a fully hydrated random coil to a dehydrated compact globule when the solution temperature is raised above the lower critical solution temperature (LCST; 32 °C) of PIPAAm, and the globule goes back to the coil below the LCST [14]. Ding et al. have reported that conjugation of PIPAAm to genetically engineering sites near the binding pocket of streptavidin yields "on–off" affinity switch that controls the binding and release of the ligand biotin through small changes in environmental conditions [15]. Similar observations were made by Yoshizako et al. in studying affinity regulations between albumin and cibacron blue (CB) using both PIPAAm and CB immobilized matrix [16]. The bound albumin on the CB was released from the matrix surface by lowering the temperature below the LCST. We have been successfully demonstrating an affinity modulation between integrins and cell adhesive Arg-Gly-Asp (RGD) sequences using RGD-functional PIPAAm-modified surfaces where the surface bioactivity can be controlled by thermal trigger [17,18]. We hypothesized that above the LCST, the grafted PIPAAm layer dehydrates and shrinks exposing the highly polar RGD sequences that can be recognized by cells. Below the LCST, on the other hand, the hydrated layer masks the immobilized peptides and diminishes the success of integrin access, resulting in cell detachment from the surface. The shielding effects of the grafted polymer layer is

* Corresponding author. Tel.: +81 3 3367 9945x6201; fax: +81 3 3359 6046.
E-mail address: tokano@abmes.twmu.ac.jp (T. Okano).

0142-9612/$ – see front matter © 2008 Elsevier Ltd. All rights reserved.
doi:10.1016/j.biomaterials.2008.05.030

thought to be one of the main factors causing cell detachment below the LCST, although there could be other factors which influence the affinity change, such as surface stiffness, hydrophilicity, ligand spacing and so on.

To disclose the shielding effects of the grafted polymer layer on integrin–RGD dissociation below the LCST, here we control a nanometer scale distance between peptides and the grafted polymer chain by employing a tether chain as a spacer, which could reduce the shielding effect of hydrated polymer layer (Fig. 1). Recent experimental studies of cell adhesion assay on bioactive bilayer membranes having both poly(ethylene glycol) (PEG) and collagen-like peptides demonstrated that human melanoma cells spread when the PEG chains are much shorter than the peptide which is fully exposed and can be recognized by cells [19]. On the other hand, when PEG chains are much longer than the peptide, they cover the ligand completely, resulting in a surface that is inert to cells. Monte Carlo simulations have also confirmed the influence of ligand branching length on the efficiency of receptor binding and the accessibility of ligands inside the polymer layer [20]. In this study, we first examined the effect of PEG tethers on cell attachment on PIPAAm-grafted surfaces above the LCST. In addition, the effect of PEG tethers on time-dependent affinity changes in integrin–RGD binding was also investigated by observing cell release kinetics from the surfaces below the LCST.

2. Materials and methods

2.1. Materials

N-Isopropylacrylamide (IPAAm) was kindly provided by Kojin Co. (Tokyo, Japan), and purified by recrystallization from *n*-hexane. 2-Carboxyisopropylacrylamide (CIPAAm) was synthesized as described previously [21]. Tissue culture grade polystylene (TCPS) dish (Falcon 3001) was purchased from Becton Dickinson Labware (Oxnard, CA). Synthetic peptides, RGD, RGDS, GRGDS, and RGES were purchased from Sigma (St. Louis, MO). Poly(ethylene glycol)-ω-amino-α-carboxyl (NH_2–PEG–COOH, 3.4 kDa) was purchased from Shearwater Co. (Huntsville, AL). 1-Ethyl-3-(3-dimethylaminopropyl)carbodiimide hydrochloride (EDC) was purchased from Dojindo Laboratories (Kumamoto, Japan). *N*-Hydroxysuccinimide (NHS) was purchased from Wako Pure Chemical Industries Ltd. (Osaka, Japan). Trypsin–EDTA solution was purchased from Gibco BRL (Grand Island, NY). Bovine aortic endothelial cells (BAECs) were provided by Health Science Research Resources Bank (JCRB 0099; Osaka, Japan). Dulbecco's modified Eagle's medium (DMEM) was purchased from Iwaki (Chiba, Japan).

2.2. Preparation of peptide-immobilized surfaces

RGD-containing peptides immobilized temperature-responsive surfaces were prepared as described previously [22]. Briefly, poly(IPAAm-co-CIPAAm) was first covalently grafted to the TCPS substrate by electron beam (EB)-induced graft polymerization (Curetron EBC-200-AA2, Nissin High Voltage Co. Ltd., Kyoto, Japan). CIPAAm was introduced as a functional group because the presence of surface functional groups is a prerequisite for the immobilization of peptides. In the grafting, 30 μl of 2-propanol solution containing IPAAm and CIPAAm was spread uniformly over surface of 35-mm TCPS dishes followed by EB irradiation. After the grafting, samples were washed with MilliQ water and kept in water at 4 °C overnight.

The immobilization of the RGD-containing peptide onto the graft polymer samples was achieved via common EDC/NHS chemistry. Briefly, the grafted polymer samples were reacted with the mixture of 2 mM EDC and 2 mM NHS. This process includes the preactivation of the surface carboxylic acid into an active ester intermediate. The samples were then washed with water and allowed to react in the RGD-containing peptide solutions (2 mM) at room temperature overnight.

In the coupling of the RGD-containing peptide to the PEG-bearing surface, a two-step peptide immobilization process was used. PEG was first end-grafted onto the poly(IPAAm-co-CIPAAm)-grafted surfaces via CIPAAm by use of EDC/NHS. The surfaces were incubated at 37 °C in the solutions containing 2.5 mM of NH_2–PEG–COOH. The reaction temperature was kept above the LCST without preventing the accessibility of PEG chains to the activated carboxyl groups. The subsequent immobilization of the peptide onto the free PEG chain ends was achieved by use of EDC/NHS. Those surfaces were rinsed with distilled water and sterilized with ethylene oxide after drying.

2.3. Cell spreading assay

BAECs were maintained in DMEM with 10% fetal bovine serum (FBS) in humidified atmosphere with 5% CO_2. Cells were passaged using 0.05% trypsin–0.26 mM EDTA in phosphate buffered saline (PBS). Cells used for adhesion studies were in passages 2–3 because cells often entered a quiescent phase and failed to proliferate after passage 5. Harvested cells were centrifuged and washed with DMEM to remove remaining serum proteins. The cell pellet was then resuspended using DMEM in the absence of FBS to yield a final concentration of 1×10^5 cells/ml and the cell suspension was plated onto the surfaces. After adding cells, the dishes were gently

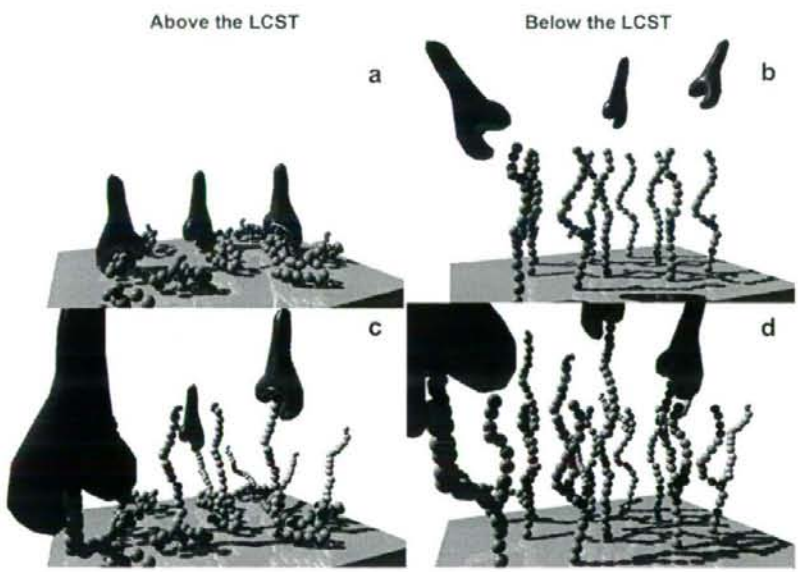

Fig. 1. Schematic views of cell adhesive peptide-bearing temperature-responsive surfaces showing thermo-induced "on–off" control of integrin–peptide binding. The grafted polymers (orange) expose tethered peptides (red) to integrins (dark blue) at "on" state above the LCST, and shield the peptides from integrin access at "off" state below the LCST (a, b). Employing extensible PEG tethers (light blue) between peptides and grafted polymer reduces the shielding effect of the protective polymer layer (c, d).

shaken to distribute the cells evenly across the substrate and placed in 5% CO_2 incubator at 37 °C for 6 or 24 h. The cell morphology was monitored and photographed under a phase contrast microscope (TE300, Nikon, Tokyo). The spread cell numbers were also counted from printed photographs and three representative fields were analyzed per dish for each surface condition ($n = 3$).

2.4. Cell detachment assay

Spread BAECs on peptide-immobilized surfaces were detached by low temperature treatment. In brief, cells were cultured on the surfaces in the absence of FBS at 37 °C for 24 h, and were transferred to a CO_2 incubator equipped with a cooling unit fixed at 20 °C. The changes in cell morphologies were continuously observed for the duration of the detachment assay and microphotographed under a phase contrast microscope. The percentage of remaining cells on the surface to the initial spread cells was presented ($n = 3$).

3. Results and discussion

3.1. Cell spreading above the LCST

Poly(IPAAm-*co*-CIPAAm) was readily grafted onto a TCPS surface by an EB irradiation method. The successful grafting of polymers onto the TCPS was determined by observing the wetting properties on the surface. The grafting of polymers made the surface more hydrophilic at 20 °C and the contact angle was less than 20°, while it was more than 50° at 37 °C as described previously [23]. The amounts of grafted polymers on the surfaces were approximately 1.8 μg/cm^2 estimated by attenuated total reflection Fourier transform infrared (ATR-FTIR), and this value corresponds to 15–20 nm of thickness as previously reported [24]. Furthermore, the hydrodynamic size of grafted poly(IPAAm-*co*-CIPAAm) copolymer was also calculated from the molecular weight of ungrafted copolymer (around 600 kDa determined by gel permeation chromatography) [25,26], and the Stokes radius value was roughly 18 nm. Plunkett et al. suggested that PIPAAm-grafted self-assembled monolayer of 19.5 nm thickness demonstrated the maximum changes in water contact angle at 25 and 37 °C [27], and these findings are consistent with our previous report, which suggested that approximately 20-nm thickness of PIPAAm layer grafted on TCPS played a crucial role in a thermo-induced cell adhesion control at the LCST [24]. Both neutron reflectivity and computational modeling of the temperature-induced structural changes of PIPAAm also indicated that the extent of chain collapse above the LCST strongly depends on the chain length and grafting density [28,29].

Fig. 2 compares cell spreadings on RGD, RGDS, GRGDS, and RGES-immobilized poly(IPAAm-*co*-CIPAAm)-grafted surfaces at 37 °C. BAECs were cultured in the absence of FBS to prevent cell adhesion by absorbed serum proteins, and the densities of spread cells were determined after 6 h of culture. Although it is likely that a fraction of the ligands could be hidden within the grafted polymer layer even above the LCST, the hydrophilic peptides were expected to expose the majority of ligands making them available to cells. For all surfaces having a RGD motif, spread cell densities were higher than those on a RGE negative control, indicating the peptide-mediated cell adhesion rather than non-specific adhesion. RGDS and GRGDS show a significant increase of cell spreading compared to RGD because the Ser occupies the position following the RGD in FN and is known as an important amino acid for the linear peptides to fit the RGD into a particular receptor [30].

Fig. 3 compares cell spreading on each of the three different peptide-immobilized surfaces as a function of CIPAAm content in feed. CIPAAm content could be corresponding with surface peptide densities, although the location of the peptides within the polymer layer is equally or more important for cell adhesion than the density (1, 3, 5, and 10 mol% of CIPAAm in the copolymer corresponds to 0.2, 0.6, 1.0, and 2.0 nmol/cm^2 at the surface peptide densities). BAECs were cultured on each surface at 37 °C for 24 h in the absence of FBS. Spread cell numbers slightly increased with CIPAAm contents, but these were not significant changes. Interestingly, the increase of cell spreading nearly saturated at 5 mol% CIPAAm which is corresponding with 1.0 nmol/cm^2 at the surface peptide density. The surfaces may have enough amounts of peptides for producing significant increase of spread cell number and the peptide spacing may be considerably smaller than the dimension of an integrin head (approximately 10 nm^2). We previously observed that the cell footprint area of individual cells correlated well with a logarithm of the peptide densities in feed [31]. Increased peptide surface density, therefore, seems to have a more influence on the formation of

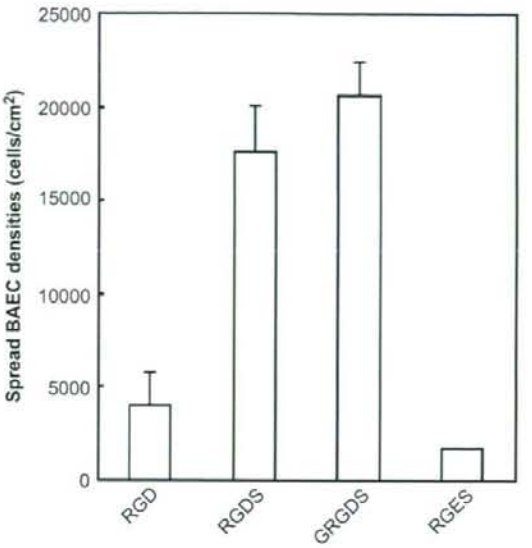

Fig. 2. Spread BAEC densities on RGD, RGDS, GRGDS, and RGES-immobilized poly(IPAAm-co-CIPAAm)-grafted surfaces (CIPAAm; 1 mol% in feed). CIPAAm is used as a linker to the peptides. BAECs were incubated at 37 °C for 6 h in the absence of FBS.

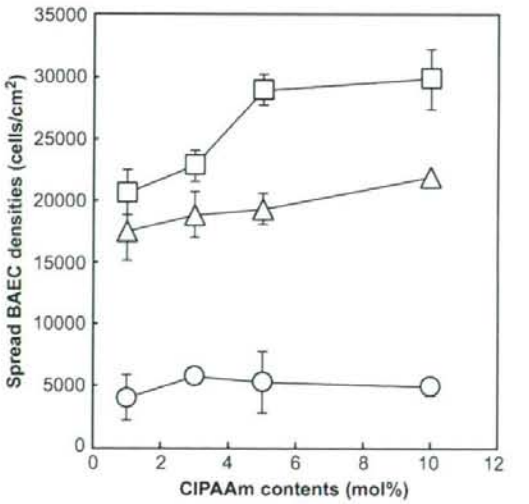

Fig. 3. Dose-dependent spreadings of BAECs on RGD (circle), RGDS (triangle), and GRGDS (square)-immobilized poly(IPAAm-co-CIPAAm)-grafted surfaces as a function of CIPAAm contents. Cells were incubated at 37 °C for 24 h in the absence of FBS.

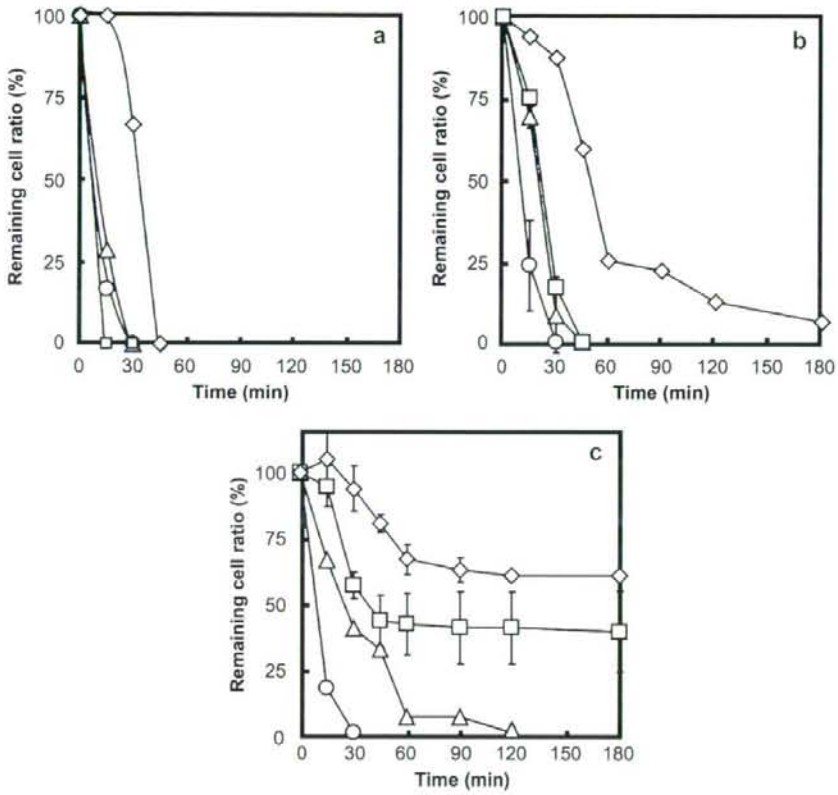

Fig. 4. Detachment profiles for BAECs seeded on RGD (a), RGDS (b), and GRGDS (c)-immobilized poly(IPAAm-*co*-CIPAAm)-grafted surfaces as a function of time (CIPAAm; 1 mol% (circle), 3 mol% (triangle), 5 mol% (square), and 10 mol% (diamond) in feed). Cells were incubated at 37 °C for 24 h in the absence of FBS, and were transferred to an incubator equipped with a cooling unit fixed at 20 °C. Results are reported as the percentage of remaining cells on the surfaces.

focal contact adhesion than spread numbers. The minimal number of integrin–RGD interactions required for cell attachment was also found to be lower than that for complete spreading [32].

3.2. Cell detachment below the LCST

Even though cell morphology apparently does not look very different, cell alters the formation of adhesive contacts with substrate in a time-dependent manner, e.g., receptor clusters and focal contact adhesion [5]. The primary advantage of using our peptide-immobilized temperature-responsive surface is that this system can provide time-dependent affinity changes in integrin–peptide binding without applying detachment forces. Our previous studies, for example, revealed that cell-surface affinity decreased with increasing cell culture time [18]. Cells start to produce ECM proteins (e.g., fibronectin, etc.) with culture time and their non-specific adsorption onto the surfaces became dominant while specific interaction between integrins and immobilized peptides were dominant at the first step of cell adhesion.

Fig. 4 compares the release kinetics of BAECs from RGD, RGDS, and GRGDS-immobilized surfaces when the culture temperature was decreased from 37 to 20 °C. The time required for cell detachment increased following the trend: RGD < RGDS < GRGDS. These results correlated well with cell spreading data (see Fig. 2). Of particular interest is that the rates of cell detachment were significantly decreased with increasing peptide densities (CIPAAm contents), whereas cell spreading numbers were not largely dependent on peptide densities as seen in Fig. 3. As mentioned above, cells may develop their affinity to the substrate depending on peptide densities, altering the formation of adhesive contacts with substrates.

3.3. Effects of PEG tethers on cell attachment/detachment

The main purpose of this study is to elucidate the mechanism of cell detachment from the peptide-immobilized surfaces below the LCST. Although the behavior of cells in contact with biomaterials was strongly influenced by the physico-chemical surface properties, such as surface wettability, roughness or chemical composition, we hypothesize that shielding of peptides by hydrated polymer layer results in decrease of peptide density available for integrin binding, followed by cell detachment from the surface. To directly address the possibility of shielding effect on cell release from the surfaces, PEG chains were used as a spacer between peptides and grafted polymer chains based on the hypothesis that employing extensible PEG chains to tethered peptides may reduce the shielding effect of PIPAAm chains.

Fig. 5 shows spread BAEC densities on PEG end-grafted poly-(IPAAm-*co*-CIPAAm) surfaces coupled and uncoupled with RGDS peptides. BAECs were cultured on each surface at 37 °C for 24 h in

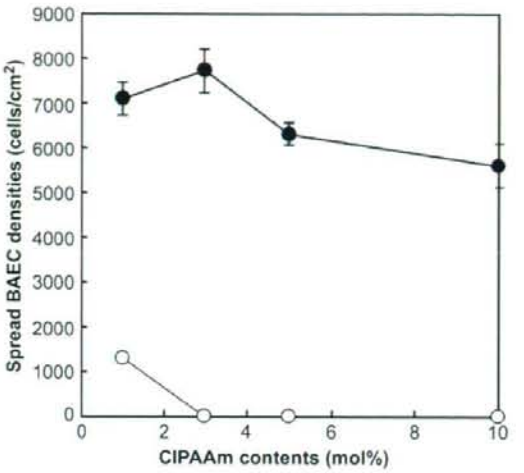

Fig. 5. Dose-dependent spreadings of BAECs on PEG-bearing poly(IPAAm-co-CIPAAm)-grafted surfaces coupled (closed) and uncoupled (open) with RGDS peptide as a function of CIPAAm contents. Cells were incubated at 37 °C for 24 h in the absence of FBS.

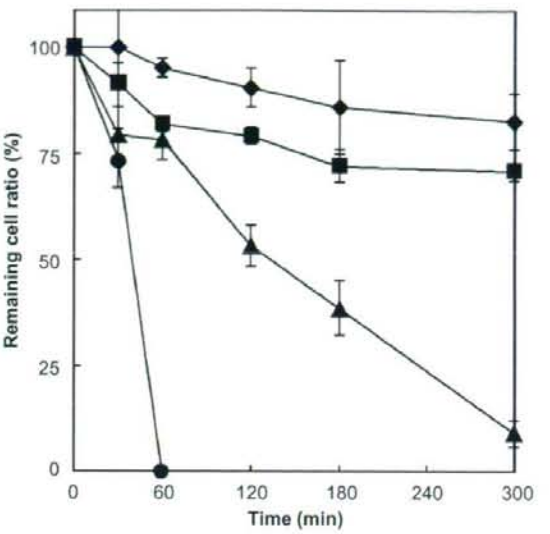

Fig. 6. Detachment profiles for BAECs seeded on RGDS-coupled PEG-bearing poly-(IPAAm-co-CIPAAm)-grafted surfaces as a function of time (CIPAAm; 1 mol% (circle), 3 mol% (triangle), 5 mol% (square), and 10 mol% (diamond) in feed). Cells were incubated at 37 °C for 24 h in the absence of FBS, and were transferred to an incubator equipped with a cooling unit fixed at 20 °C. Results are reported as the percentage of remaining cells on the surfaces.

the absence of FBS. Cells plated on the uncoupled sample remained predominantly rounded and no spreadings were observed when CIPAAm content was more than 3 mol%. This reason is that grafted PEG numbers could increase with increasing CIPAAm contents. Many studies suggested that PEG modified surfaces are non-adhesive to cells due to a steric repulsive force, etc. [33]. Also, unsubstituted carboxyl groups also could make the surface non-adhesive to cells. In contrast, cell spreadings were observed on the surfaces where RGDS peptides were coupled to the free PEG chain ends. The spread cell densities, however, were not as high as those on RGDS-coupled surfaces without PEG tethers (see Fig. 3), despite the extensible PEG chains were expected to encourage cells to recognize the tethered peptides enhancing the ligand availability. It is plausible that unsubstituted PEG chain ends making the surface non-adhesive to cells. Also, the flexible PEG spacers could lead to increased ligand mobility and reduced ligand–integrin affinity. In any case, these results indicate that RGDS peptides were successfully coupled to the PEG chain ends for integrin-mediated cell attachment.

Cell detachment assay revealed a more pronounced effect of PEG tethers. Fig. 6 demonstrates the release kinetics of BAECs from RGDS-coupled PEG-grafted surfaces when the culture temperature was decreased from 37 to 20 °C. As expected, the time required to release cells from the surface was found to be longer when peptides were coupled to an extensible tether ends. Interestingly, the rates of cell detachment were significantly decreased with increasing peptide densities (CIPAAm contents), whereas cell spreading numbers were not largely dependent on peptide densities as seen in Fig. 5. In the sample with 10 mol% of CIPAAm, more than 80% of cells have still retained on the surface within the timeframe measured, while almost all the cells were released after 180 min when peptides were not tethered with PEG (see Fig. 4B). From these results, the observed retarded behavior in cell release kinetics is most likely due to the extension of tethered RGDS by inserted PEG chains, encouraging cells to recognize the tethered RGDS even below the LCST.

As with avidin–biotin interactions, integrin–RGD interaction occurs over a very short range and architectural change on the nanometer length scale is crucial for controlling integrin–RGD binding. Cells are known to form and break integrin–RGD bonds dramatically during adhesion and thus, the successful "on–off" affinity control of integrin–RGD binding may be attributed to the weak binding energy of integrin–RGD bonds compared to other biological bonds. The length of ligand-coupled tethers significantly influence receptor-mediated interactions in the presented system. These observations indicate that an appropriate nano-distance between cell adhesive peptides and the grafted polymers is crucial for thermo-induced "on–off" integrin recognition.

4. Conclusions

A detail mechanism of thermo-induced cell detachment from RGD peptide-coupled temperature-responsive polymer-grafted surfaces was investigated. Temperature-responsive polymer was readily grafted onto TCPS surfaces by an EB irradiation method. RGD-containing peptides were successfully immobilized onto the grafted surface via amide bond through the reaction between the amino group of the peptide and an activated surface carboxyl group. The significant increase of cell adhesion on RGD-containing substrates was observed at "on" state above the LCST, indicating that the cell-substrate interaction is highly RGD specific. When temperature was decreased below the LCST (inactive "off" state), cells started to come off from the surface. The time required to release cells from the surface was, however, found to be longer when peptides were coupled to an extensible tether ends. This increases the exposure of the RGD sequence toward the cells, leading to active "on" state even below the LCST. Together with previous findings, these results indicate that the shielding effect of the grafted polymer layer is thought to be one of the main factors causing cell detachment below the LCST. This study contributes to the fundamental understanding of ligand–receptor recognitions.

Acknowledgments

The work was supported in part by a Grant-in-Aid for Scientific Research on Priority Area (Grant No. 17076014), the High-Tech

Research Center Program, the Center of Excellence (COE) Program for the 21st Century, and the Formation of Innovation Center for Fusion of Advanced Technologies in the Special Coordination Funds for Promoting Science and Technology, from the Ministry of Education, Culture, Sports, Science and Technology (MEXT), Japan.

References

[1] Sako Y, Minoghchi S, Yanagida T. Single-molecule imaging of EGFR signaling on the surface of living cells. Nat Cell Biol 2000;2:168–72.
[2] Miyamoto S, Teramoto H, Gutkind JS, Yamada KM. Integrin can collaborate with growth factors for phospharylation of receptor tyrosine kinases and MAP kinase activation: roles of integrin aggregation and occupancy of receptors. J Cell Biol 1996;135:1633–42.
[3] Stayton PS. May the force be with you. Nature 1999;397:20–1.
[4] Xiong JP, Stehle T, Diefenbach B, Zhang R, Dunker R, Scott DL, et al. Crystal structure of the extracellular segment of integrin $\alpha_v\beta_3$. Science 2001; 294:339–45.
[5] Baneyx G, Baugh L, Vogel V. Fibronectin extension and unfolding within cell matrix fibrils controlled by cytoskeletal tension. Proc Natl Acad Sci U S A 2002; 99:5139–43.
[6] Miyamoto S, Akiyama SK, Yamada KM. Synergistic roles for receptor occupancy and aggregation in integrin transmembrane function. Science 1995;267: 883–5.
[7] Dejana E, Colella S, Conforti G, Abbadini M, Gaboli M, Marchisio PC. Fibronectin and vitronectin regulate the organization of their respective Arg-Gly-Asp adhesion receptors in cultured human endothelial cells. J Cell Biol 1988; 107:1215–23.
[8] Palecek SP, Loftus JC, Ginsberg MH, Lauffenburger DA, Horwitz AF. Integrin–ligand binding properties govern cell migration speed through cell-substratum adhesiveness. Nature 1997;385:537–40.
[9] Geiger B, Bershadsky A, Pankov R, Yamada KM. Transmembrane extracellular matrix-cytoskeleton crosstalk. Nat Rev Mol Cell Biol 2001;2:793–805.
[10] Cukierman E, Pankov R, Stevens DR, Yamada KM. Taking cell-matrix adhesions to the third dimension. Science 2001;294:1708–12.
[11] Shimoboji T, Larenas E, Fowler T, Hoffman AS, Stayton PS. Temperature-induced switching of enzyme activity with smart polymer–enzyme conjugates. Bioconjug Chem 2003;14:517–25.
[12] Shimoboji T, Larenas E, Fowler T, Kulkarni S, Hoffman AS, Stayton PS. Photoresponsive polymer–enzyme switches. Proc Natl Acad Sci U S A 2002;99: 16592–6.
[13] Shimoboji T, Ding ZL, Stayton PS, Hoffman AS. Photoswitching of ligand association with a photoresponsive polymer–protein conjugate. Bioconjug Chem 2002;13:915–9.
[14] Fujishige S. Intrinsic viscosity–molecular weight relationships for poly(*N*-isopropylacrylamide) solutions. Polym J 1987;19:297–300.
[15] Ding Z, Fong RB, Long CJ, Stayton PS, Hoffman AS. Size-dependent control of the binding of biotinylated proteins to streptavidin using a polymer shield. Nature 2001;411:59–62.
[16] Yoshizako K, Akiyama Y, Yamanaka H, Shinohara Y, Hasegawa Y, Kikuchi A, et al. Regulation of protein binding toward a ligand on chromatographic matrixes by masking and forced-releasing effects using thermoresponsive polymer. Anal Chem 2002;74:4160–6.
[17] Ebara M, Yamato M, Aoyagi T, Kikuchi A, Sakai K, Okano T. A novel approach to observing synergy effects of PHSRN on integrin–RGD binding using intelligent surfaces. Adv Mater, in press.
[18] Ebara M, Yamato M, Aoyagi T, Kikuchi A, Sakai K, Okano T. Temperature-responsive cell culture surfaces enable "on–off" affinity control between cell integrins and RGDS ligands. Biomacromolecules 2004;5:505–10.
[19] Dori Y, Bianco-Peled H, Satija SK, Fields GB, McCarthy JB, Tirrell M. Ligand accessibility as means to control cell response to bioactive bilayer membranes. J Biomed Mater Res 2000;50:75–81.
[20] Chen CC, Dormidontova EE. Architectural and structural optimization of the protective polymer layer for enhanced targeting. Langmuir 2005;21:5605–15.
[21] Aoyagi T, Ebara M, Sakai K, Sakurai Y, Okano T. Novel bifunctional polymer with reactivity and temperature sensitivity. J Biomater Sci Polym Ed 2000;11: 101–10.
[22] Ebara M, Yamato M, Hirose M, Aoyagi T, Kikuchi A, Sakai K, et al. Copolymerization of 2-carboxyisopropylacrylamide with *N*-isopropylacrylamide accelerates cell detachment from grafted surfaces by reducing temperature. Biomacromolecules 2003;4:344–9.
[23] Ebara M, Yamato M, Nagai S, Aoyagi T, Kikuchi A, Sakai K, et al. Incorporation of new carboxylate functionalized co-monomers to temperature-responsive polymer-grafted cell culture surfaces. Surf Sci 2004;570:134–41.
[24] Akiyama Y, Kikuchi A, Yamato M, Okano T. Ultrathin poly(*N*-isopropylacrylamide) grafted layer on polystyrene surfaces for cell adhesion/detachment control. Langmuir 2004;20:5506–11.
[25] Tiktopulo EI, Uversky VN, Lushchik VB, Klenin SI, Bychokova VE, Ptitsyn OB. "Domain" coil-globule transition in homopolymers. Macromolecules 1995;28: 7519–24.
[26] Tanford C. Protein denaturation. Adv Protein Chem 1968;23:121–282.
[27] Plunkett KN, Zhu X, Moore JS, Leckband DE. PNIPAM chain collapse depends on the molecular weight and grafting density. Langmuir 2006;22:4259–66.
[28] Yim H, Kent MS, Huber DL, Satija S, Majewski J, Smith GS. Conformation of end-tethered PNIPAM chains in water and in acetone by neutron reflectivity. Macromolecules 2003;36:5244–51.
[29] Mendez S, Curro JG, McCoy JD, Lopez GP. Computational modeling of the temperature-induced structural changes of tethered poly(*N*-isopropylacrylamide) with self-consistent field theory. Macromolecules 2005;38: 174–81.
[30] Assa-Munt N, Jia X, Laakkonen P, Ruoslahti E. Solution structures and integrin binding activities of an RGD peptide with two isomers. Biochemistry 2001;40: 2373–8.
[31] Ebara M, Yamato M, Aoyagi T, Kikuchi A, Sakai K, Okano T. Immobilization of cell-adhesive peptides to temperature-responsive surfaces facilitates both serum-free cell adhesion and noninvasive cell harvest. Tissue Eng 2004;10: 1125–35.
[32] Massia SP, Hubbell JA. An RGD spacing of 440 nm is sufficient for integrin alphaV beta3-mediated fibroblast spreading and 140 nm for focal contact and stress fiber formation. J Cell Biol 1991;114:1089–100.
[33] Szleifer I. Protein adsorption on surfaces with grafted polymers: a theoretical approach. Biophys J 1997;72:595–612.

JOURNAL OF TISSUE ENGINEERING AND REGENERATIVE MEDICINE
J Tissue Eng Regen Med 2008; **2**: 190–195.
Published online in Wiley InterScience (www.interscience.wiley.com) **DOI:** 10.1002/term.80

RESEARCH ARTICLE

Transportation of transplantable cell sheets fabricated with temperature-responsive culture surfaces for regenerative medicine

Takayuki Nozaki[1,2], Masayuki Yamato[2], Toshiaki Inuma[3], Kohji Nishida[4] and Teruo Okano[2]*
[1]*Advanced Research Laboratory, Hitachi Ltd, 2520 Akanuma, Hiki-gun Hatoyama-cho, Saitama 350-0395, Japan*
[2]*Institute of Advanced Biomedical Engineering and Science, Tokyo Women's Medical University, 8-1 Kawada-cho, Shinjuku-ku, Tokyo, Japan*
[3]*Corporate Logistics Technology Office, Hitachi Transport System Ltd, 7-2-18 Toyo, Koto-ku, Tokyo 135-8372, Japan*
[4]*Department of Ophthalmology, Tohoku University School of Medicine, 1-1 Seiryo-cho, Aoba-ku, Miyagi 980-8574, Japan*

Abstract

Here we report transportation of cell sheets fabricated on temperature-responsive culture surfaces for regenerative medicine. On the surfaces cells adhere, spread and proliferate at 37 °C, but upon temperature reduction below 32 °C all the cells are spontaneously detached. When cells on the surfaces are challenged by long distance transportation, maintaining the temperature is critical. Therefore, we developed a portable homothermal container to keep the inner temperature at 36 °C for >30 h without any need for batteries or energy supply. We transported and compared fibroblast sheets cultured on temperature-responsive surfaces in the container, at room temperature in a car, or on ice. After 8 h transportation by car, all cells at room temperature and on ice were detached from the surfaces and some were folded and broken into tiny pieces. On the other hand, fibroblast sheets transported in the container retained their adhesion to the dish surfaces and intact cell sheets were successfully harvested by temperature reduction. During the transportation, cell viability and histology were not impaired. This unique transportation device would be useful for cell sheet-based regenerative medicine utilizing temperature-responsive culture surfaces. Copyright © 2008 John Wiley & Sons, Ltd.

Received 8 January 2008; Accepted 11 March 2008

Keywords cell sheet; transportation; container; fibroblast; temperature-responsive; cell viability

1. Introduction

We have developed a novel technology based on cell sheets fabricated on temperature-responsive culture surfaces, cell sheet engineering for regenerative medicine (Yang *et al.*, 2006). By utilizing cell sheet engineering, we have already succeeded in clinical applications to treat human patients with carrier-free cell sheets in skin (Yamato *et al.*, 2001) and cornea (Nishida *et al.*, 2004). In order to fabricate transplantable carrier-free cell sheets, we developed temperature-responsive culture surfaces (Yamada *et al.*, 1990). Since a temperature-responsive polymer, poly(*N*-isopropylacrylamide), is covalently immobilized, these surfaces facilitate cell adhesion, spreading and growth at 37 °C, but the cells are detached from the surfaces upon temperature reduction below the polymer's lower critical solution temperature of 32 °C, without the need for proteolytic enzymes such as trypsin. Therefore, all the confluent cells are harvested as a single contiguous cell sheet, and harvested cell sheets retain the intact extracellular matrix deposited during culture (Kushida *et al.*, 1999; Yamato *et al.*, 2001) as well as membrane proteins, including cell–cell junctional proteins and growth factor receptors, and ion channels (Kushida *et al.*, 2001, 2005). Therefore, these cell sheets rapidly reattach onto other surfaces, such as host tissues.

*Correspondence to: Teruo Okano, Institute of Advanced Biomedical Engineering and Science, Tokyo Women's Medical University, 8-1 Kawada-cho, Shinjuku-ku, Tokyo 162-8666, Japan. E-mail: tokano@abmes.twmu.ac.jp

At present, transplantable cell sheets are fabricated in a GMP (Good Manufacturing Practices)-grade CPC (cell processing centre) of our hospitals, and applied to patients in the same hospitals. But fabricated cell sheets can be expected to be shipped out from our CPC to other hospitals in the near future. In order to achieve such cell sheet delivery, we developed a portable homothermal container designed for transportation of cell sheets fabricated on temperature-responsive culture surfaces. To prevent unexpected cell detachment from temperature-responsive culture surfaces, this device was designed to keep the inner temperature close to 37 °C without any energy supply during the whole transportation period.

2. Materials and methods

2.1. Cell culture

Rat dermal fibroblasts were isolated from 6–10 week-old male Wister rats. Briefly, rat skin was excised from the back using scissors and treated with 1000 U/ml dispase II (Godo Shusei, Tokyo, Japan) in Dulbecco's modified Eagle's medium (DMEM) at 37 °C for 3 h. Epidermis was peeled off under a dissecting microscope, and cut into small pieces using scissors. The tissues obtained were treated with 0.2% collagenase I (Wako, Osaka, Japan) in DMEM at 37 °C with shaking. All the solution containing small tissue pieces was then filtred through a 0.22 μm pore filter, and centrifuged at 1500 r.p.m. for 5 min. Precipitates were resuspended with DMEM containing 10% fetal bovine serum. The dermal fibroblasts btained were seeded onto tissue culture polystyrene dishes and cultured for cell expansion. After some passages, fibroblasts were finally seeded onto square-patterned temperature-responsive culture dishes (60 mm diameter; CellSeed Inc., Tokyo, Japan) at an initial density of 2.5×10^4 cells/cm^2. On the dishes, a square temperature-responsive culture domain (24 × 24 mm) is surrounded by a non-cell adhesive domain grafted with polyacrylamide and cultured at 37 °C. After 1 week of culture, the fibroblasts reached confluency. Before transportation experiments, we checked whether these cell sheets could be successfully harvested by reducing the temperature. These confluent fibroblasts were detached from the temperature-responsive culture dishes within 30 min after temperature reduction to 20 °C, and square fibroblast sheets were obtained.

2.2. Transportation

One day prior to the transportation experiments, the culture medium was changed. All the dishes were sealed with Parafilm (Pechiney Plastic Packaging Inc, Chicago, IL, USA) to avoid CO_2 diffusion and pouring of culture medium. As a positive control (Group A), some dishes with confluent fibroblasts were kept in an incubator (37 °C, 5% CO_2). Other groups were transported by car for 8 h. A newly developed portable container was used for Group B. In Groups C and D, the dishes were kept at room temperature in a car and on ice, respectively. Temperature was continuously monitored during transportation. The transportation experiments were performed in triplicate.

2.3. Evaluation

Recovered cell sheets were fixed with 10% formalin (Wako Chemicals), and embedded in paraffin wax. Sections (4–5 μm) were stained with haematoxylin and eosin (H&E) or Azan. Cell activity was evaluated with a fluorogenic esterase substrate, calcein AM, and dead cells were detected with ethidium homodimer-1 (Invitrogen, Carlsbad, CA, USA). Nuclei were stained with Hoechst 33 342. Stained cells were observed under a fluorescence microscope equipped with a digital camera. Cell viability was evaluated as follows:

$$\text{Viability} = (N_{\text{Hoechst}} - N_{\text{dead}})/N_{\text{Hoechst}} \times 100\%$$

where N_{Hoechst} represents the total cell number positively stained with Hoechst 33 342 and N_{dead} represents the number of dead cells positively stained with ethidium homodimer-1.

3. Results

A portable homothermal container (30 cm in diameter of the top, 27.5 cm in height) that allows transport with a constant inner temperature at 36 °C was newly developed to prevent cell sheet detachment from temperature-responsive culture surfaces (Figure 1a). The wall of the container has vacuum heat insulation to minimize heat loss (Figure 1b). At the core of the homothermal container, a small inner chamber (15 cm in sides, 5 cm in height, Figure 1c) was installed, and the top and bottom of the inner chamber were directly contacted by copper plates to make heat distribution uniform. The inner chamber was filled with a heat storage material, *n*-eicosane, in plastic bags (Figure 1d). Temperature-responsive culture dishes were placed at the centre of the inner chamber during transportation and surrounded by the heat storage material. The top and bottom of the copper plates were planarly contacted with two boxes (15 cm in sides, 3 cm in height) filled with the heat storage material. The extra space inside the portable container was occupied by an adiabator to reduce heat loss.

Since the melting temperature of *n*-eicosane is 36.4 °C and the heat storage material was prewarmed in a thermostat at 37 °C before use, the inner temperature is kept around 36 °C during transportation. To evaluate the requisite amount of heat material to keep the inside temperature around 36 °C, time-dependent heat distribution was simulated with heat fluid analysing computer software (STAR-CD, CD-Adapco, London, UK;

DOI: 10.1002/term

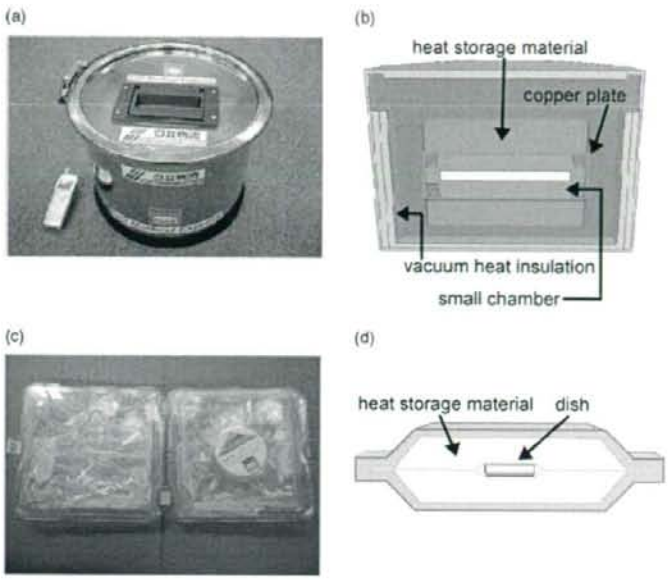

Figure 1. A portable homothermal container for cell and tissue transportation. (a) Its appearance. Note a cell phone by the container as a scale. (b) Its inner structure. (c) A small chamber for culture dishes. (d) Cross-sectional view of the chamber containing a culture dish at the core

Figure 2). When 920 g heat storage material is stored in the container, the material solidified within 9 h, but the inner temperature of the inner chamber was kept around 36 °C for >30 h (data not shown).

Then, the temperature change was measured. During the melting of the heat storage material, the inner temperature of the small chamber was kept stable at 36 °C. When the container was placed outside (16–24 °C) in Spring of Japan, the inner temperature declined below 35.8 °C after 37.9 ± 3.7 h ($n = 4$, Figure 3a). Even in a cold room (4 °C), the inner temperature was maintained at 36 °C for 18.2 ± 0.8 h ($n = 4$, Figure 3b). After the lid of the container was opened to take out the dishes and the container inside was exposed to room temperature (23–25 °C) for 1 min, the inner temperature transiently decreased to 32 °C, but the inner temperature was recovered to 36 °C within 4 min after the lid was closed again ($n = 4$, Figure 3c).

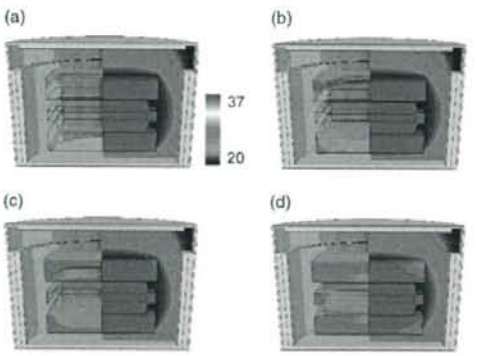

Figure 2. Computer simulation of heat distribution. The initial temperature of the heat storage material and the inner chamber was 36.4 °C. Each panel shows (a) 45 min, (b) 100 min, (c) 5 h, (d) 9 h after the exposure to ambient temperature at 20 °C. The left side of each panel shows solidification of heat storage material, in which blue colour depicts the solidified heat storage material. The right side shows the inner heat distribution

With the portable container, fibroblast sheets fabricated on temperature-responsive culture surfaces were transported for 8 h by car under the following three conditions: in the container (Group B), at room temperature in a car (Group C), and on ice (Group D). Group A was a positive control without transportation; the dishes of this group were just stored in a CO_2 incubator at 37 °C. The portable container could keep the inner temperature at 36.1 ± 0.1 °C (Group B, Figure 4), although the outer temperature was significantly changed. Dishes transported without the portable container at room temperature in a car (Group C) and on ice (Group D) experienced 20–30 °C and 5–10 °C, respectively.

Dishes of Group A stored in a CO_2 incubator at 37 °C for 8 h were moved to another CO_2 incubator at 20 °C. Within 30 min, all the cells were detached from the temperature-responsive culture dishes as a single contiguous cell sheet, then shrank in size after floating in the culture medium (Figure 5a), as observed with other cell types (Murakami *et al.*, 2006; Shimizu *et al.*, 2002). Even after the 8 h transportation, all the cells of Group B still intactly adhered to the temperature-responsive culture dishes and no cell morphological changes were observed. Then,

DOI: 10.1002/term

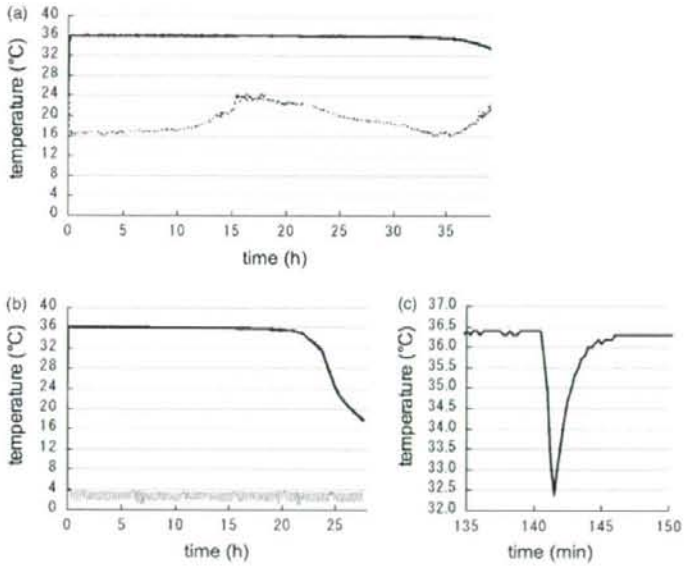

Figure 3. Temperature change of the inner chamber in the homothermal container. (a) Temperature inside the inner chamber (solid line) and under ambient temperature in Spring of Japan (dotted line). (b) Temperature inside the inner chamber (solid line) and temperature of a cold room where the container was placed (dotted line). (c) Quick recovery of the inner chamber temperature after the lid was opened for 1 min

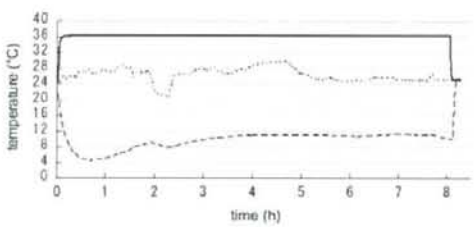

Figure 4. Temperature change of the inner chamber in the homothermal container during 8 h transportation by car. Each line shows temperature inside the inner chamber (solid line, corresponding to Group B), the room temperature inside the car (dotted line, corresponding to Group C), or the temperature observed with a thermocouple probe close to the ice (dashed line, corresponding to Group D)

these cells were challenged to temperature reduction to 20 °C. All the cells were detached from the dishes as a single contiguous cell sheet within 30 min and shrank, as observed with Group A (Figure 5b). In contrast, all the cells in Groups C and D were detached as cell sheets during the transportation (Figure 5c–e). Some cell sheets folded or were broken into pieces (Figure 5c, e). By histological evaluation with H&E and Azan staining, significant differences were not observed between Groups A and B (Figure 6). Fragments of detached cell sheets of Groups C and D also showed similar histology to them, implying the absence of severe cellular damages. Cells of Groups A and B were subjected to cell viability tests immediately after 8 h incubation at 37 °C and transportation, respectively (Figure 7). The cell viabilities were >97% ($n = 3$) in both groups.

4. Discussion

In the present study, a novel portable homothermal container was developed. This container does not need batteries or an energy supply to keep the inner temperature at 36 °C. The obtained results with carrying fibroblasts on temperature-responsive culture dishes showed that cell viability was maintained during the 8 h transportation by car, and finally transplantable fibroblast sheets were successfully harvested from the dishes upon temperature reduction. Although the container does not have a function to maintain CO_2 concentration, the pH was successfully maintained during the transportation by making culture dishes full of culture medium and sealing with Parafilm. Another concern was oxygen supply. In the present setting, no oxygen was supplied to the culture medium during transportation. Therefore, when other cell types that consume more oxygen are transported for longer distances, lack of oxygen can be a problem. However, rabbit primary corneal epithelial cells that were stratified on culture dishes were also challenged to transportation in the same fashion, but did not show any damage during the transportation (data not shown).

In order to make regenerative medicine more widespread, novel infrastructures need to be developed. For example, all the processes including cell isolation,

DOI: 10.1002/term

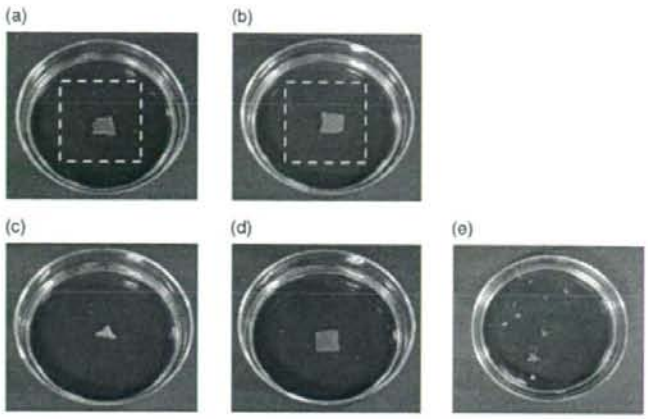

Figure 5. Fibroblast sheets after 8 h transportation. (a) Transplantable fibroblast sheets harvested by temperature reduction to 20 °C after 8 h incubation in a 5% CO_2 incubator at 37 °C as a positive control (Group A). (b) Transplantable fibroblast sheets harvested by temperature reduction after 8 h transportation within the portable homothermal container (Group B). Dashed squares depict the shapes of fibroblast sheets attached on the surfaces of temperature-responsive culture dishes before low temperature treatment. Floating fibroblast sheets detached during 8 h transportation at room temperature in the car (Group C) (c) and on ice (Group D) (d). Sometimes, cell sheets detached during transportation were broken into pieces during transportation (e)

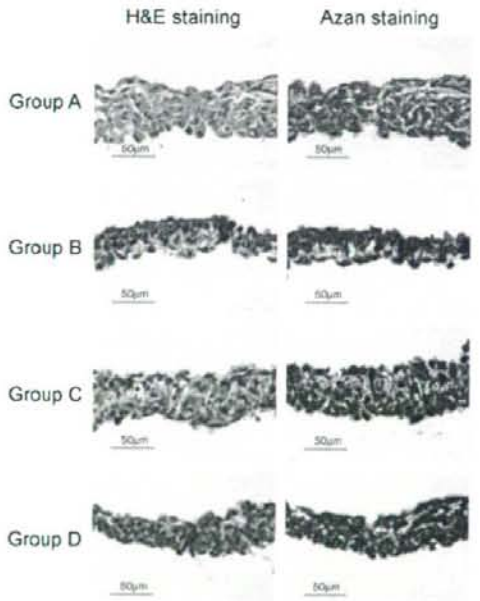

Figure 6. Histology of cell sheets. Cell sheets harvested after 8 h incubation in a 5% CO_2 incubator (Group A) or transportation within the portable homothermal container (Group B) and those detached during transportation at room temperature in a car (Group C) or on ice (Group D) were histologically examined

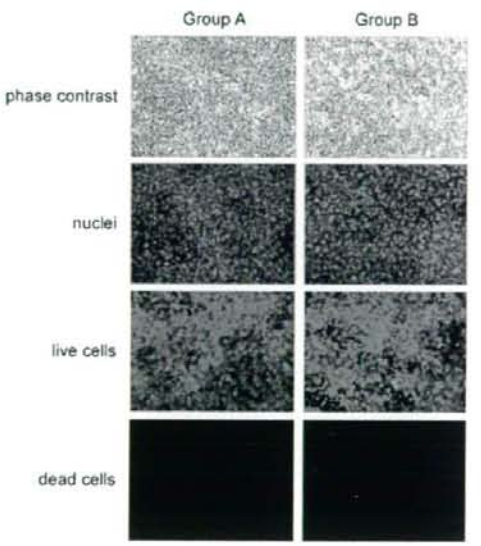

Figure 7. Cell viability test. Cells were fluorescently triple-stained with a DNA-staining dye (all nuclei), calcein AM (live cells) and ethidium homodimer-1 (dead cells) after 8 h incubation in a 5% CO_2 incubator (Group A) or transportation within the portable homothermal container (Group B)

seeding, medium change and monitoring are manually performed by well-trained technicians in a GMP-grade CPC to prevent contamination and achieve quality control. In the future, these manual manipulations and expensive facilities would be replaced by automated factories, as observed with automobile and semiconductor factories. We believe that transportation is another key issue as the infrastructure. With well-developed transportation technology, tissue-engineered products can be shipped out from the central CPC, not only to neighborhoods but also to distant hospitals and overseas, resulting in the increase of opportunities for clinical applications of regenerative medicine to patients.